공학박사학위논문

**Flow Dynamics of Highly Elastic Fluids in 4:1 Microcontraction Channel**

4:1 수축 미세 유로를 흐르는 탄성 유체의 흐름에 관한 연구

2014년 8월

서울대학교 대학원

화학 생물 공학부

이대웅

# 4:1 수축 미세 유로를 흐르는 탄성 유체의 흐름에 관한 연구

## Flow Dynamics of Highly Elastic Fluids in 4:1 Microcontraction Channel

지도교수 안 경 현

이 논문을 공학박사 학위논문으로 제출함

2014년 5월

서울대학교 대학원

화학생물 공학부

이대웅

이대웅의 박사학위논문을 인준함

2014년 6월

위 원 장_____(인)

부위원장_____(인)

위    원_____(인)

위    원_____(인)

위    원_____(인)

# ABSTRACT

## Flow Dynamics of Highly Elastic Fluids

## in 4:1 Microcontraction Channel

Lee, Daewoong

School of Chemical and Biological Engineering

The Graduate School

Seoul National University

The structure of viscoelastic flow through contraction geometry has been one of the benchmark problems in rheology. Especially, formation of vortex is very important issue. Vortex is not a desirable phenomenon in practical applications such as polymer processing. It causes defects in products with the residence time of material. So there have been many investigations of dynamics of vortex in contraction geometry to understand it. However, there was only little attention given to the dynamics of purely elastic flows in contraction channel, particularly, unstable flows caused by elasticity. In this thesis, sequence of flow patterns developed by elasticity was investigated. Moreover, the phenomenon in transition state, before reaching steady state, and the dynamics of flows after steady state were studied.

Three main goals have been pursued in this thesis. The first objective of this study was to figure out the structure of elastic flow in contraction geometries. The flow patterns of viscoelastic fluids flowing inside 4:1 planar contraction microchannels were investigated and quantitatively analyzed. Micro-devices enhanced the elastic effects with theirs small dimension, and they can also easily monitor the flows with high resolution visualization technique. A wide range of Weissenberg number ($Wi$) flows of poly(ethylene oxide) solutions were observed while maintaining low Reynolds number ($O(10^{-2}) > Re$). The flow pattern changed from a Newtonian-like flow to a flow with a vortex growth region, during which a divergent flow and lip vortex were also observed depending on the elasticity number ($El$) and aspect ratio. The flow pattern in the contraction microchannel was found to be diverse and abundant depending on the aspect ratio and elasticity number. (Chapter 3)

In the second part of the study, the relationship between transient flow behavior at high $Wi$ and steady state flows at lower $Wi$ was verified to establish time-$Wi$ superposition experimentally. As the Weissenberg number ($Wi$) increased, the flow developed from a Newtonian-like flow to vortex growth, and the transient start-up flow at high $Wi$ was found to experience all the steady patterns at lower $Wi$ flows. The flow sequence was different depending on the fluids and channel dimensions as above. However, in all of the cases we could reach, the steady patterns at each low $Wi$ flow could be matched 1:1 with the transient patterns at each high $Wi$ flow. The plot of $Wi$ and time when the two sets (transient and

steady) were matched showed a clear functional relationship, from which the time-Weissenberg number superposition could be confirmed. (Chapter 4)

As the last part of thesis, dynamics of unstable flows were examined and characterized. In chapter 3 & 4, the flows were stable. However, as the Weissenberg number increased, by increasing either the shear rates or the elasticity of the fluids, the vortex fluctuated with a certain period. To reach the unstable state, highly elastic fluids ($M_w$=5$\times$10$^6$ g mol$^{-1}$, PEO solutions) were used. In unstable flows, the vortex fluctuates constantly. At first it oscillates with certain periods, it is oscillating vortex. The oscillating vortex was symmetric at first and became asymmetric with various patterns. As the elasticity increased further, the vortex randomly fluctuated without any certain time period. The Lyapunov exponent for the change in vortex size was positive, meaning that the flow was spatially chaotic. (Chapter 5)

This thesis systematically analyzed the flow patterns of the elastic fluids in the micro-contraction flow, which included; Newtonian-like flow, divergent flow, steady vortex growth, oscillating flow with symmetry, oscillating flow with asymmetry, and chaotic flow.

*Keywords*: microfluidics, contraction geometry, viscoelastic flow, aspect ratio, time-Weissenberg number superposition, unstable flows

**Student Number:** 2009-30245

**CONTENTS**

# LIST OF TABLES

# LIST OF FIGURES

# 1. Introduction

## 1.1. Flow dynamics in contraction geometry

The flow behavior of viscoelastic fluids is important not only in classical polymer processing but also in new technologies such as ink jet printing, so the study of this topic is motivated largely in processing operations. (Boger 1987) Understanding the mechanism of diverse flow dynamics for the non-Newtonian fluids depending on their condition (such as flow rate, channel geometry or properties of fluid) is an important issue for those processes to control the process. So there are a lot of studies about viscoelastic flows to make high quality products with high throughput (Hertel & Münstedt 2008). Especially, the contraction flows of viscoelastic fluids are one of the benchmark problems in rheology. Contraction and expansion geometry is inevitable in most of processing operations, and vortex enhancement is an important characteristic of viscoelastic flows in contraction geometry. Vortex formation is detrimental to the industrial processes because it causes waste of the resins and limitation on the production rates when the materials, particularly polymeric materials,rotate in vortex for a long time (Chiba et al. 1995; Haste 2007).

Therefore, there have been many studies about viscoelastic contraction flows (Boger 1987; White et al. 1987; Chiba et al. 1992; Owen & Phillips 2002; Boger & Walters 1993; Nigen & Walters 2002). Vortex could be generated with Newtonian fluids in contraction geometry under certain condition (Viriyayuthakorn & Caswell 1980; Boger et al. 1986), but viscoelastic fluid forms distinctive flow patterns,

including vortex, under wider range of flow conditions. When the flow rate or the elasticity of a fluid is small, the flow pattern is fairly simple and easy to control. However, as the shear rate or the elasticity increases, vortex enhancement is observed, and many distinct flow patterns appear (Boger 1997; Nigen & Walters 2002; Cable & Boger 1978, 1979; Nguyen & Boger 1979; Walters & Webster 1982). The mechanism behind the formation of these diverse flow patterns is still unclear because it is affected by number of parameters such as channel geometry, shear rate and fluid elasticity. The effect of these parameters have been covered with many experimental studies: the rheological properties of the fluids, contraction shape (abrupt, tapered, rounded, and hyperbolic), types of contraction (planar, square, and axisymmetric), flow rate, contraction ratio (Boger 1986; McKinley et al. 1991; Rodd et al. 2005; Rodd et al. 2007; Evans & Walters 1986; Evans & Walters 1989; Rothstein & McKinley 2001; Rodd et al. 2005; Schuberth & Münstedt 2008; Alves et al. 2008; Yesilata et al. 1999; Yesilata et al. 2000; Cogswell 1972; Yasuda & Sugiura 2008; McKinley et al. 2007; Oliviera et al. 2007; Sousa et al. 2009).

The main purpose of studying viscoelastic flow dynamics in contraction geometry under number of circumstances as above is to predict and understand the kinematics of flow, especially, when elasticity increased. Flow patterns, such as vortex enhancement, have been observed by various methods like laser-Doppler velocimetry (LDV), particle tracking velocimetry, and long-exposure images (Lawler et al. 1986; Raiford et al. 1989; Santiago et al. 1998; Raffel et al. 1998; Meinhart et al. 1999; Alves et al. 2008; Rodd et al. 2007; Dembek 1982). These flow-visualization methods can be divided into nonintrusive method like hot wire or pressure tube and intrusive

method using probes, and also can be divided into indirect or direct methods. In this study, particle streak image technique, which is intrusive and direct, was used to capture exact visual of flow patterns, even in unstable flows.

Many of above studies have investigated the viscoelastic flows, and the flow instability from the elasticity of fluid has received special attention. Among above factors that affect flow conditions, the effect of elasticity has been the focus not only for the flow in the contraction geometry but also for many other flows. In particular, there has been much interest in flow instability which is caused by purely elastic flow characteristics. There have been many studies on the effect of elasticity on flow patterns inside contraction channels (Pakdel & Mckinley 1996; Bonn & Meunier 1997; Kwon 2012; Kwon & Park 2012). In those studies, polymer solutions were used to induce elastic instability. When experiments were performed with elastic fluids with a simple shear flow, curved streamlines were observed at a low shear rate unlike Newtonian fluids. Depending on the type of polymer, the pattern for the streamline changed, from which the effect of elasticity on flow instability could be deduced. Groisman reported how the mechanism of flow destabilization by elasticity is different from that of inertia (Groisman & Steinberg 1998).

Studies on contraction flows have mostly been done with macro scale channels (i.e. channel size was on the order of millimeters or larger). Macro channels have advantages in dealing with highly viscoelastic fluids. However, it is not easy to generate a high shear rate with devices using such a large length scale. In addition, it is difficult to observe the purely elastic effect because the Reynolds number also becomes large at a high shear rate. It becomes hard to distinguish whether flow

instability comes from elasticity or from inertia.

Therefore, it can be advantageous to use microfluidic devices, in which a high deformation rates can be attained while maintaining a low Reynolds number. In other words, a high Weissenberg number (characteristic time of the fluid ($\lambda$) multiplied by the characteristic shear rate ($\dot{\gamma}$), $Wi = \lambda\dot{\gamma}$) flow could be explored while maintaining a low Reynolds number due to the small scale length of the microchannel. The effect of elasticity on flow could be observed while keeping the inertial effect minimal (Groisman & Quake 2004; Mitchell 2001; Whitesides 2006; Rodd et al. 2005; Rodd et al. 2007; Gulati et al. 2008). Diverse flow patterns including vortex formation caused by elasticity at a high Weissenberg number have been reported by both experiments and simulations. (Rodd et al. 2005; Rodd et al. 2007; Alfonso et al. 2011) In addition, the Elasticity number ($El = Wi/Re$), which is the Reynolds number divided by the Weissenberg number, has also been used to explain such a diverse flow development in microchannel studies (Rodd et al. 2007).

Flow dynamics, especially vortex, in sudden contraction has been also a classical benchmark problem in computational studies (Owen & Phillips 2002; Alves 2008), and many simulations were also performed in an effort to understand the dynamics of a highly elastic flow with low Reynolds number (Alfonso 2011). It was demonstrated by both experiment and simulation that a vortex is formed with a high Weissenberg number even when there is no inertial force.

In the contraction flow for the macro-size, also in numerical simulation, a lip vortex often appeared as the Weissenberg number increased. However, in planar

contraction channels whose width is on the order of tens or hundreds of micrometers, there have been many cases where a lip vortex did not appear and a unique flow pattern called a divergent flow appeared. A divergent flow is the flow in which the location of the maximum flow velocity is not right above the point of the contraction but is moved upstream due to fluid elasticity, resulting in a distortion of the flow. This phenomenon was also demonstrated in a simulation using the upper-convected Maxwell (UCM) model (Alves & Poole 2007).

Most of the previous studies have focused on the flow patterns at steady states, while experimental studies on the transient behavior have rarely been performed. There are some simulations about transient of start-up flow in contraction or constriction (contraction-extension) geometry. Bishko et al. calculated how vortex formed when the viscoelastic fluid flows though a 4:1 contraction geometry at various Weissenberg number. There also exists a study on the transient behavior, in which the center of the vortex changes its motion when the pressure drop changes to slow growth in the start-up flow (Szabo et al. 1997). Kim et al. performed a numerical study and reported that the transient flow at a certain Weissenberg number experienced all the steady flow patterns at lower Weissenberg numbers, and suggested the principle of superposition of the time and the Weissenberg number. In their graph of the time-Weissenberg number superposition, the slope changed at the point where the lip vortex and the corner vortex merged.

There have been also experimental studies about transient flows in contraction geometry. The flow characteristics of polymer solutions were studied experimentally

by McKinley et al. in terms of the Deborah number ($De = \lambda / \tau$) which is defined as the relaxation time of the fluid ($\lambda$) divided by the processing time ($\tau$). When the velocity profile was measured near the contraction, it fluctuated due to the change in elasticity even when no significant external change was observed. Depending on the Deborah number and the contraction ratio, the velocity fluctuation was either periodic or non-periodic, and a map of the flow regimes could be drawn. They analyzed the fluctuation of the velocity profile due to the elasticity. The flow pattern was in a steady state with a steady streamline over time, and only the flow velocity fluctuated due to elasticity. The unsteady state in which the vortex was fluctuating was not studied in detail. In the studies where macro-size contraction geometry was used, the flows with high Weissenberg numbers could not be reached due to the limitation of the shear rate, and flow dynamics has been studied mostly in steady states. There were some reports on the vortex oscillation that arises due to elasticity (Yesilata et al. 1999; Alves, et al. 2005; Kwon 2012).

In all the above studies, flow dynamics in contraction geometry has been studied extensively. However, detailed characteristics or the flow patterns in the unsteady region, caused purely by the elasticity of the fluid, have not been explored yet even in micro-scale devices. Because flow behaviors like vortex enhancement could be observed without using highly elastic liquids, dilute polymer solutions have been widely used. While Rodd et al. dealt with the time-dependent diverging flow, most researches have not covered unsteady flow dynamics such as the vortex fluctuation after the steady vortex.

## 1.2. Outline of the thesis

The objectives of this study are to examine and characterize diverse flow patterns of viscoelastic fluids inside micro-fabricated 4:1 contraction planar channels. Not just the flow patterns or the formation of the vortex but also sequence of flow enhancement were observed. The flow patterns developed from a Newtonian-like flow to a flow with a vortex growth regime in which the corner vortex grew as the Weissenberg number increased. The flow development was affected by various flow conditions.

In section 3, to understand the effects of the channel aspect ratio and elasticity number among the many factors, the changes in flow patterns were observed and analyzed with various micro-channels of constant height and different sizes and with fluids of different elasticity.

In section 4, all the transient flow patterns at the initial high Weissenberg number flow were compared and matched to the flow patterns at steady states at lower Weissenberg numbers by changing the fluid elasticity and the channel dimension. By doing this, whether the time-Weissenberg number superposition, which was proposed by numerical simulation, was a principle involved in the complexity of this flow or simply was just the result of numerical artifact was examined.

In section 5, the flow pattern as well as its change over a wide range of Elasticity number and Weissenberg number was studied through flow visualization, and systematical analysis of the flow profiles was performed. Especially, highly elastic fluids and one smaller dimension channel were used to get high Weissenberg

number flows, while keeping the Reynolds number small ($O(10^{-2}) > Re$). With those, even unstable flows, caused by elasticity, were quantitatively analyzed.

# 2. Experimental Section

## 2.1. Fluids

Polyethylene oxide (PEO) which is a commonly used water-soluble polymer was used in this study. Various polyethylene oxide (PEO, Sigma Aldrich, USA) solutions were prepared with two different molecular weights: 0.3wt%, 0.4 wt%, 0.5 wt%, 0.6 wt%, 0.7 wt% and 1.0 wt% (molecular weight of $2{\times}10^6$ g mol$^{-1}$), 0.4wt%, 0.6wt%, 0.7wt%, 0.8wt%, and 1.0wt% (molecular weight $5{\times}10^6$ g mol$^{-1}$)

These solutions were applied to 4:1 microcontraction geometries for investigating various flow patterns. The steady shear viscosity of each solution was measured using a strain-controlled rheometer (ARES, TA Instruments, USA) with 60mm parallel plates at 25℃. The viscosity curves as a function of the shear-rate are shown in Figure 2.1 and 2,2. Solutions of Figure 2.1 were used for section 3, and solutions of Figure 2.2 were used for section 4 and 5. The zero-shear viscosities, obtained by fitting with the Carreau model:

$$\eta = \eta_0[1+(\lambda\dot{\gamma})^2]^{(n-1)/2}, \tag{2.1}$$

The relaxation time was measured using a capillary breakup extensional rheometry (CaBER), which is appropriate for the measurement of low viscosity polymer solutions. (Rodd et al. 2004) The zero-shear viscosity and the relaxation time of each solution are provided in Table 2.1 and Table 2.2. The range of relaxation times for the solutions measured by CaBER were $14 < \lambda < 82$ ms, and the zero-shear viscosity was in the range of $0.009 < \eta_0 < 39 \, Pa \cdot s$. All solutions showed shear thinning at high

shear rates.
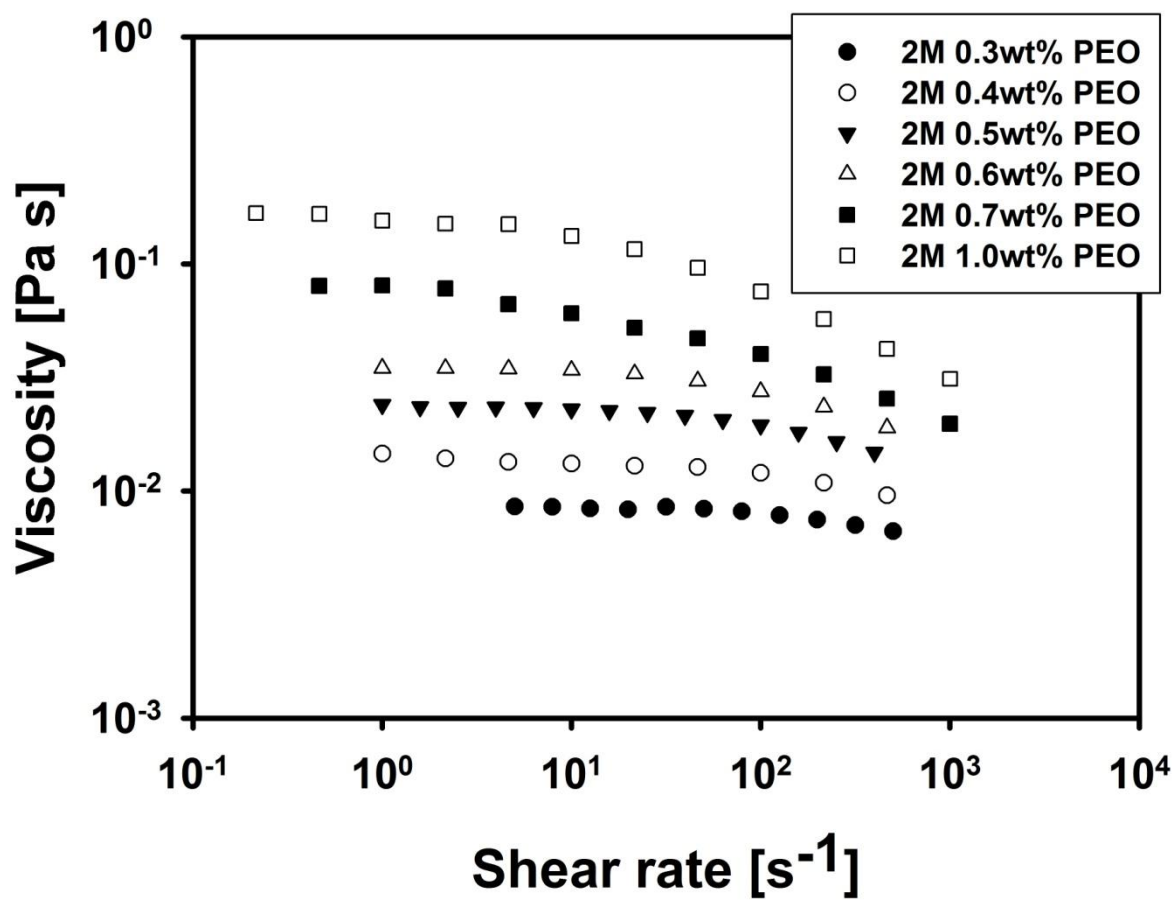
**Figure 2.1.** Steady shear viscosity data for 0.3 wt%, 0.4 wt%, 0.5 wt%, 0.6 wt%, 0.7 wt% and 1.0 wt% ($M_w$=2×$10^6$ g mol$^{-1}$) PEO solutions.
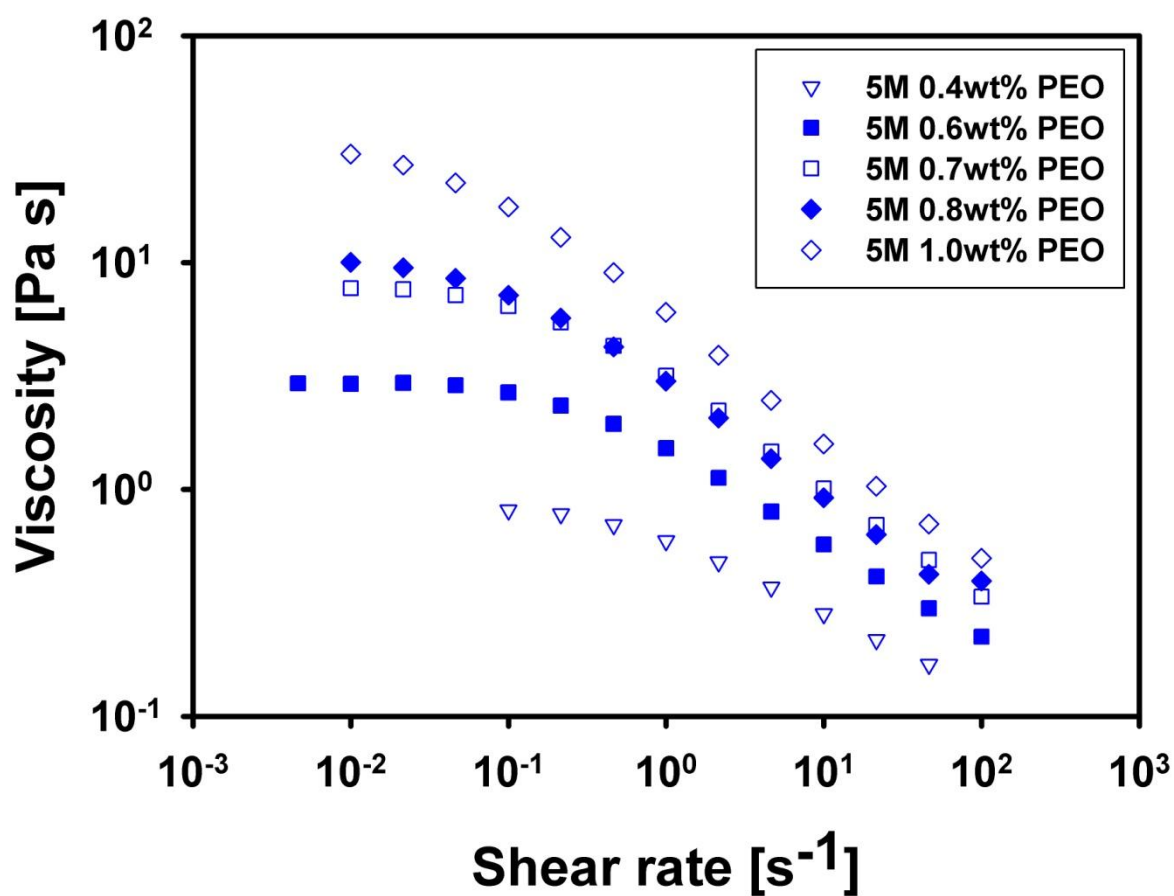
**Figure 2.2.** Steady shear viscosity data for 0.4 wt%, 0.6 wt%, 0.7 wt%, 0.8 wt% and 1.0 wt% ($M_w$=5×10$^6$ g mol$^{-1}$) PEO solutions.

**Table 2.1.** Rheological properties of solutions at 25℃. (PEO of $M_w = 2 \times 10^6$ g mol$^{-1}$)

| PEO concentration | 0.3 wt% | 0.4 wt% | 0.5 wt% | 0.6 wt% | 0.7 wt% | 1.0 wt% |
|---|---|---|---|---|---|---|
| $\eta_0$ (Pa・s) | 0.009 | 0.015 | 0.026 | 0.035 | 0.055 | 0.20 |
| $\lambda$ (s) | 14 | 16 | 18 | 20 | 22 | 25 |

**Table 2.2.** Rheological properties of solutions at 25℃. (PEO of $M_w = 5 \times 10^6$ g mol$^{-1}$)

| PEO concentration | 5M 0.4wt% | 5M 0.6wt% | 5M 0.7wt% | 5M 0.8wt% | 5M 1.0wt% |
|---|---|---|---|---|---|
| $\eta_0$ (Pa・s) | 0.81 | 3.5 | 7.7 | 8.2 | 39 |
| $\lambda$ (ms) | 46 | 46 | 50 | 52 | 82 |

## 2.2. Micro devices

The experiments were performed in a 4:1 planar contraction channel with the following dimensions. They are six contraction channels, with schematics shown in Figure 2.3 (a), and the channel size, listed in Table 2.3, was from 160 μm : 40 μm to 800 μm : 200 μm. The height of the channels was fixed at 70 μm for all the channels. In this manner, the aspect ratio of the channels ($\Lambda$), defined by the ratio of the height to the upstream width ($w_u$), could be varied from 0.068 to 0.438.

To observe the effect of the aspect ratio of the channel on the change in flow pattern and universality of time-Weissenberg number superposition, experiments were performed with channels of different size. The direction of flow is $-y$. Figure 2.3 (b) shows a microscopic image of cross-sectional view. Corner angle was nearly 90° with range of 88° < angle < 91°.

The channel was constructed using poly(dimethylsiloxane) (PDMS, Sylgard 184A, Dow Corning), with a mold made with thick photo-resist (SU-8 50, MicroChem Corp., USA) and high-resolution chrome mask. (McDonald et al. 2000; Anderson et al. 2000; Whitesides & Stroock 2001; Strook & Whitesides 2002; Rodd 2006) SU-8 was spin coated with a uniform thickness onto a silicon wafer, and the mold was patterned by soft-lithography of the chrome mask. PDMS was poured over the pattern and the transparent PDMS channel was obtained after heating in an oven. The experiments were performed using these channels attached to a cover glass which was thinly coated by PDMS at a thickness of 5 to 7 μm. The ratio of the PDMS to the

curing agent (Sylgard 184B, Dow Corning) was 10:1. Each part (the channel and the PDMS-coated cover glass) were baked in oven at 80°C for 30 min, and then baking bonded channel in oven at 80°C over 24 hours. The adhesive strength of the PDMS coated cover glass was higher than that of a piece of cover glass with no surface treatment. Thus, the channel made with the PDMS coated cover glass showed improved durability, and the four walls in the channel had the same hydrophobicity.

(a)



88 - 91°
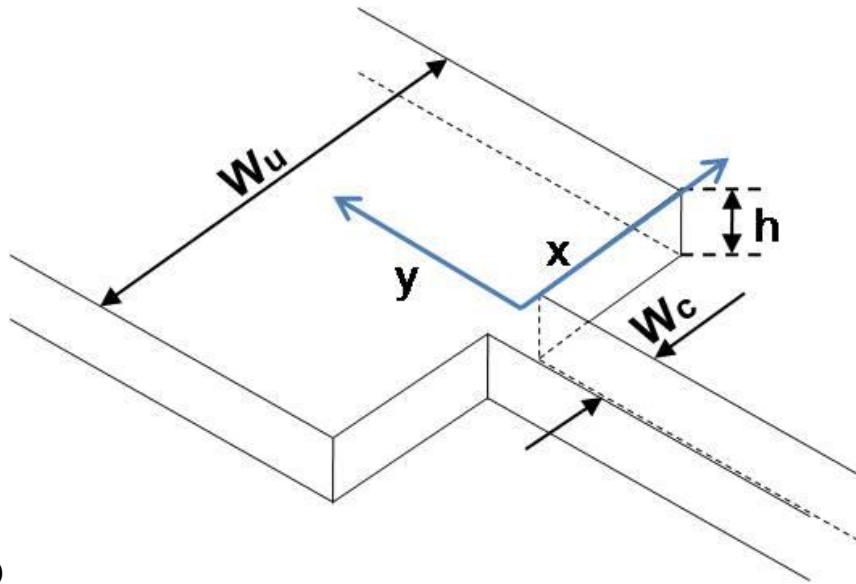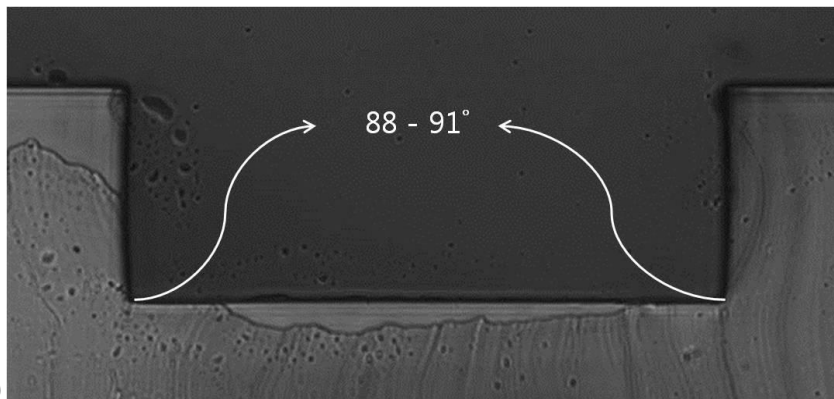
(b)

**Figure 2.3.** (a) A schematic of the 4:1 sudden contraction geometry: $w_u$ = upstream width of channel, $w_c$ = width of contraction, $h$ = depth of channel. (b) Photo of cross-section of the actual channel 3.

**Table 2.3.** Dimensions of the channels.

| | $w_u : w_c$ | $h$ | Aspect ratio $\Lambda = h/w_u$ | Magnification |
|---|---|---|---|---|
| Channel 1 | 160μm:40μm | | 0.34 | x20 |
| Channel 2 | 180μm:45μm | | 0.30 | x20 |
| Channel 3 | 200μm:50μm | 50 - 55 μm | 0.27 | x20 |
| Channel 4 | 400μm:100μm | | 0.13 | x10 |
| Channel 5 | 600μm:150μm | | 0.091 | x10 |
| Channel 6 | 800μm:200μm | | 0.068 | x4 |

## 2.3. Visualization

To visualize the flows through 4:1 contraction channels, particle streak imaging method was used. A schematic of the imaging setup was shown in Figure 2.4. For flow visualization, 0.02wt% red fluorescent particles (Molecular Probes FluoSpheres, Introvigen Corp., USA) with a 1.0 μm diameter (excitation/emission = 520/580 nm) were dispersed throughout the fluid. A mercury lamp (IX-71, Olympus, Japan) and a filter (XF102-2, Omega optical) were used to continuously illuminate 530 – 590 nm wavelength light. A highly sensitive CCD camera (EM-CCD C9100, Hamamatsu, Japan) and image processing software (HCImage, Hamamatsu, Japan) were used to capture images at 1000 x 1000 pixels and 30.00 fps. (Rodd et al. 2005)

In order to adjust the changes in image size due to the variation in channel size, different magnification lenses were used as described in Table 2.3. To achieve the best resolution images, magnification from the microscope body was also used when it is possible. Channel 6 was quite bigger than usual microcontraction channel, (Rodd et al. 2007; Dendukuri et al. 2007; Kang et al. 2005) so 4X objective lens was used for proper visualization. The flow was from the wide upstream part to the narrow downstream part. As shown in Figure 2.3, the length of the upstream part from the inlet to the contraction was 1 cm, and the length of the downstream part was 3 cm. The length of the downstream part affected the vortex formation in the upstream part, and the downstream part was designed to be much longer than that of the upstream part to minimize this effect. (Rodd et al. 2010)
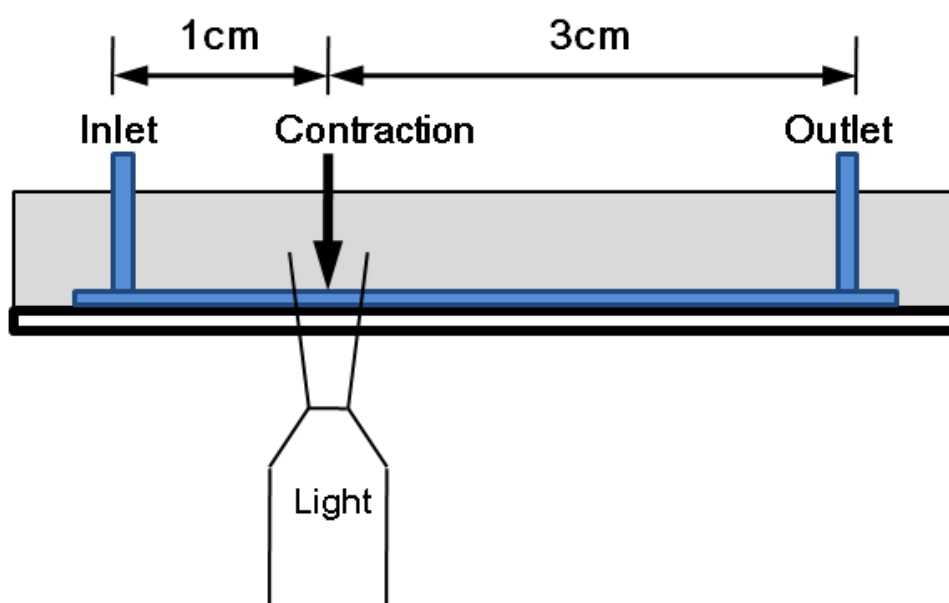
**Figure 2.4.** A schematic of fluorescent streak imaging setup.

## 2.4. Flow rate control

The fluids were supplied to microchannels with 1 ml or 2.5 ml glass syringe (GASLIGHT, Hamilton, USA). Syringes were connected to inlet of microchannels with flexible Teflon tubing (inner diameter 0.5mm) through stainless steel capillary. There was no treatment for outlet of channels. Flow rate was controlled by syringe pump (PHD2200, Harvard Apparatus, USA) in range 0f 0.5 – 15 ml/hr.

## 2.5. Dimensionless numbers

In this thesis, the following dimensionless quantities were defined in order to characterize the flow dynamics inside the microchannel (Rodd et al. 2005): the Reynolds number ( $Re$ ), the Weissenberg number ( $Wi$ ), and the Elasticity number ( $El$ ).

$$Wi = \lambda \bar{\gamma}_c = \frac{\lambda V_c}{w_c / 2} = \frac{\lambda Q}{h w_c^2 / 2} \qquad \text{- (2.1)}$$

$$Re = \frac{\rho \bar{V}_c D_h}{\eta_0} = \frac{2\rho Q}{(w_c + h)\eta_0} \qquad \text{- (2.2)}$$

$$El = \frac{Wi}{Re} = \frac{2\lambda\eta}{\rho w_c D_h} = \frac{\lambda\eta(w_c + h)}{\rho w_c^2 h} \qquad \text{- (2.3)}$$

where $\lambda$, $\bar{\gamma}_c$, $Q$, $w_c$, $h$, $\rho$, $\bar{V}_c$, $\eta_0$, $D_h$ represent the relaxation time of the fluid, the average shear-rate at contraction throat, the volumetric flow rate, the contraction width, the channel depth, the fluid density, the average flow velocity, the zero-shear viscosity, and the hydraulic diameter, respectively. $D_h$ was defined by

$$D_h = 2w_c h(w+h)$$

$Wi$ is the product of the shear rate at the contraction part and the relaxation time of the solution. This quantity is a dimensionless number, which represents the deformation rate that the fluid experiences during the flow. $Wi$ is widely used for flows, such as the simple shear flow, that have a constant stretch history. In the microchannel, a high $Wi$ can easily be attained because the shear is large. $Re$ is the ratio between the inertial force and the viscous force in the flow, and it is much smaller than $10^{-1}$ in the microchannels which were used in this study. So it does not affect the flow condition significantly. These two dimensionless numbers are affected by the flow kinematics and increase with an increase in the volumetric flow rate $Q$. However the Elasticity number, $El$, which is defined as the ratio of elastic stress and the inertial stress, is not affected by the flow kinematics and depends only on the fluid characteristics and channel geometry. When various fluids and different microchannels are used as in this thesis, the $El$ can be used to represent different experimental setups.

# 3. Flow dynamics in microcontraction geometry

## 3.1. Method of experiment

Although different fluids and channels were used in this study, the experiments could be well-organized using only the $El$ and the aspect ratio of the channel. The flow dynamics was observed by changing the two parameters mentioned above. The six different PEO solutions given in Figure 2.1 were allowed to flow at different flow rates inside six channels of different size as described in Table 2.3. The sequence of the flow patterns was organized with the increase in flow rates. From this, the entire flow pattern of the viscoelastic flow in the micro-contraction channels was classified as we increased the shear rate and fluid elasticity. Although the order of pattern formation did not change in any of the flow experiments, there were cases where certain flow patterns did not appear. The effects of the aspect ratio of the channel and the elasticity number in the flow pattern were analyzed.

## 3.2. General sequence of flow development

The flow patterns inside the micro-contraction channels were investigated, and the flow instabilities observed at different shear rates and fluid elasticity were systematically compared. The resulting flow patterns are shown in Figure 3.1 in the order of their development. As shown in this figure, the flow inside the 4:1 micro-fabricated channel exhibited various flow patterns depending on the $El$ and $Wi$. In

the micro-scale devices, it was very difficult to observe Newtonian fluids forming a complex flow pattern.

The viscoelastic PEO solution also exhibited only a Newtonian-like flow (A) when the elasticity or the flow rate was low. When the elasticity was slightly increased from the previous case, a lip vortex (B) appeared. This vortex expanded towards the side wall and resulted in a corner vortex (C). The corner vortex disappeared as the flow rate was further increased,so it is called weak vortex. With an increase in flow rate, a divergent flow (D) was observed in which the flow streamline was distorted to form a bulbous shape in which the maximum velocity occurred not at the contraction part but further upstream. (Rodd et al. 2007; Alves & Poole 2007) A schematic of the divergent flow is shown in Figure 3.2. Divergent flow can be identified with the centerline velocity. In divergent flow, it shows divergent throat and divergent bulb. Divergent throat is the part that streamlines became narrow, after that part streamlines get bulge like a bulb.

When the elasticity was increased further, the vortex growth region (E), in which the size of the steady corner vortex increased, was reached. The flow regimes discussed so far were steady states. When the shear rate or the fluid elasticity was increased further, the flow became unstable. Unstable state will be described minutely in section 5.

**Figure 3.1.** Sequence of the overall flow development in the 4:1 planar micro-contraction channel.
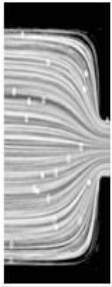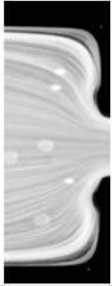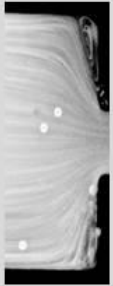
(A) Newtonian-like flow

(B) Lip vortex

(C) Weak vortex

(D) Divergent flow

(E) Vortex growth
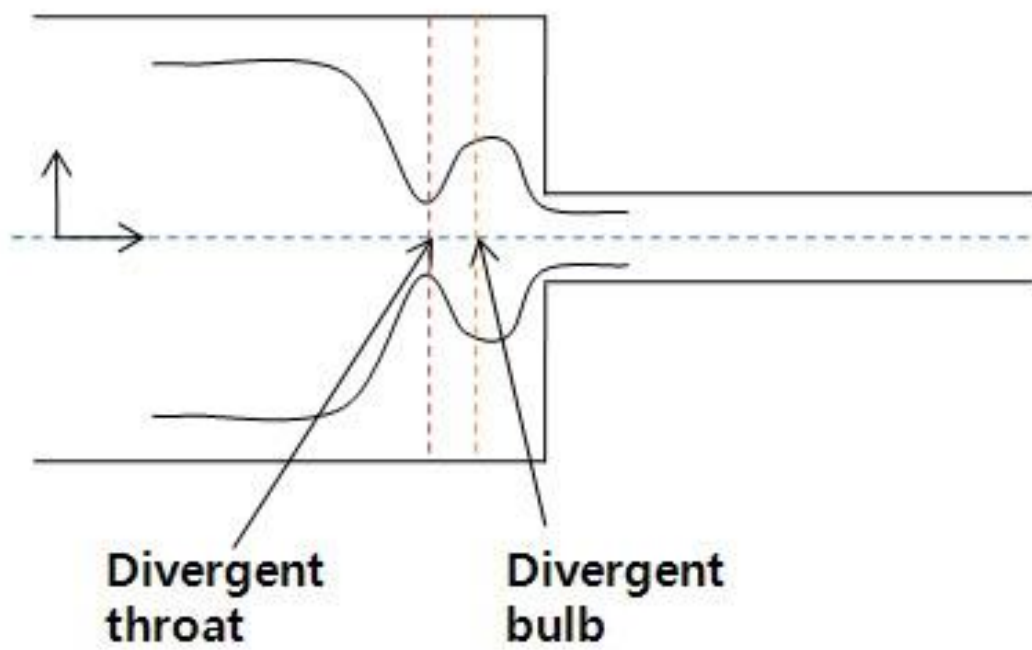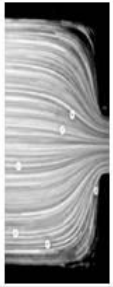
**Figure 3.2.** A simple feature of divergent flow.

## 3.3. Effect of aspect ratio and El on vortex dynamics

The flow pattern was analyzed from the flows of the different PEO solutions in different channels with varying aspect ratios. When the flow rate was increased, the formation of the flow pattern shown in Figure 3.1 was observed 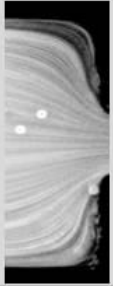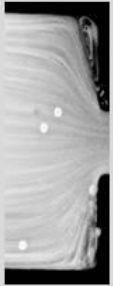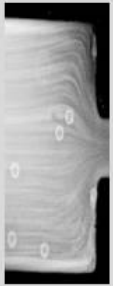in the same sequence for all the solutions. Some of the flow patterns were not observed in some cases depending on the aspect ratio of the channel or the elasticity number. However, the order of the pattern formation never changed. For example, the weak vortex (C) before the divergent flow was not observed for low aspect ratio channel 5 (600 μm : 150 μm). In the channels with a high aspect ratio, such as channel 3 and the smaller ones, the lip vortex (B) appeared only for very limited flow conditions. However, even in such a case, a change in the order of sequence, for example a corner vortex developing first and then turning into a lip vortex, never occurred.

The difference in flow sequence in terms of the aspect ratio of the channel is shown in Figure 3.3. For the channels with an aspect ratio smaller than 0.13 (channels 4, 5, and 6), the lip vortex always appeared. However, the divergent flow sometimes did not appear depending on the fluid elasticity, and the corner vortex never appeared. When the channel aspect ratio was larger than 0.25 (channels 1, 2, and 3), all the flow patterns were observed. However, except for the Newtonian-like flow and the vortex growth regime, the flow patterns exhibited a difference dependent on the $El$.

The flow pattern was affected not only by the aspect ratio but also by the elasticity number. (Rodd et al. 2007) The difference in flow patterns in terms of $El$ is

| | Newtonian-like flow | Lip vortex | Weak vortex | Divergent flow | Vortex growth |
|---|---|---|---|---|---|
| Aspect ratio Low, Λ≤0.13 | $Wi=6.9$ | $Wi=55.6$ | | $Wi=111.1$ | $Wi=208.3$ |
| Aspect ratio High, Λ≥0.25 | $Wi=7.4$ | $Wi=59.2$ | $Wi=103.5$ | $Wi=162.7$ | $Wi=124.1$ |

**Figure 3.3.** Flow sequence depending on the aspect ratio of the channel. ($\Lambda \geq 0.25$, Channels 1, 2, 3; $\Lambda \leq 0.13$, Channels 4, 5, 6).
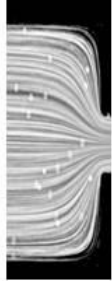
shown in Figures 3.4 and 3.5. For the channels with an aspect ratio less than 0.13 (channels 4, 5, and 6), two different sequences were observed as shown in Figure 3.4. For the case where $El$ was smaller than 30, the divergent flow was always observed regardless of the channel size. However, when $El$ was on the order of several hundreds, the lip vortex transformed into a corner vortex and continued to expand. In other words, the lip vortex disappeared, and the divergent flow appeared for a small $El$. However, the lip vortex never disappeared but the vortex just continued to expand when $El$ was large.
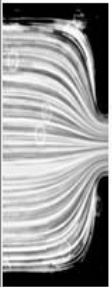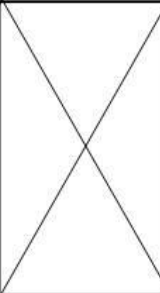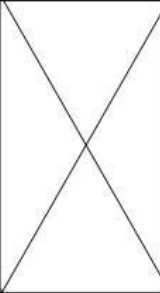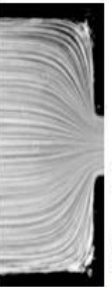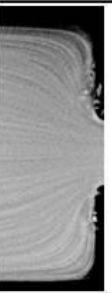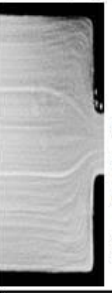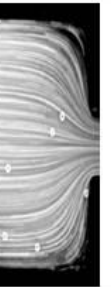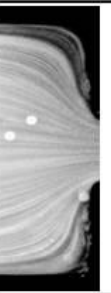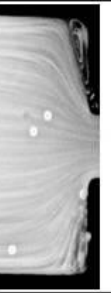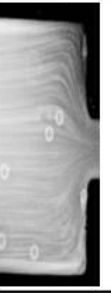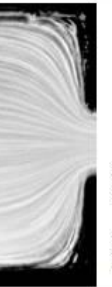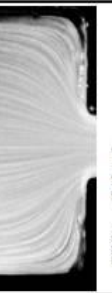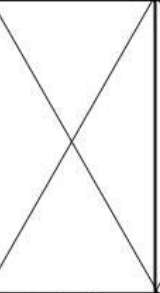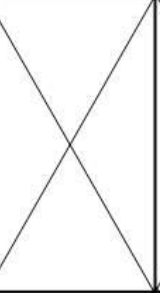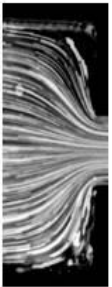
When the aspect ratio was larger than 0.25, the flow developed in more diverse ways. Figure 3.5 shows the flow sequence in a high aspect ratio channel. All of the flows showed the same pattern as a Newtonian-like flow at a low $Wi$ and a vortex growth region where the corner vortex increased in size at high $Wi$. However, the flow patterns between these two regions were diverse.

The results are organized into a single map shown in Figure 3.6. As seen in the figure, there was a critical aspect ratio between 0.13 and 0.25 where the flow sequence changed significantly. Even for the flows at the same aspect ratio, the change in $El$ caused a variation in the sequence of the flow patterns.

| | Newtonian-like flow | Lip vortex | Weak vortex | Divergent flow | Vortex growth |
|---|---|---|---|---|---|
| Elasticity number Low (El=30) | $Wi=6.9$ | $Wi=55.6$ | | $Wi=111.1$ | $Wi=208.3$ |
| Elasticity number High (El=800) | $Wi=3.4$ | $Wi=11.3$ | | | $Wi=34.0$ |

**Figure 3.4.** Flow sequence in the low aspect ratio channels. ($El$=30, Channel 4 with 2M 0.3 wt% PEO; $El$ =800, Channel 5 with 2M 1.0 wt% PEO).

| | Newtonian-like flow | Lip vortex | Weak vortex | Divergent flow | Vortex growth |
|---|---|---|---|---|---|
| $El$=90 (0.3 wt%) | $Wi$=5.6 | | | $Wi$=138.9 | |
| $El$=170 (0.4 wt%) | $Wi$=6.5 | $Wi$=65.5 | | $Wi$=131.0 | |
| $El$=360 (0.5 wt%) | $Wi$=7.4 | $Wi$=59.2 | $Wi$=103.5 | $Wi$=162.7 | |
| $El$=540 (0.6 wt%) | $Wi$=8.2 | $Wi$=32.8 | | | $Wi$=81.9 |
| $El$=900 (0.7 wt%) | $Wi$=8.9 | | | | $Wi$=124.1 |

**Figure 3.5.** Flow patterns in channel 3 with various elasticity numbers.
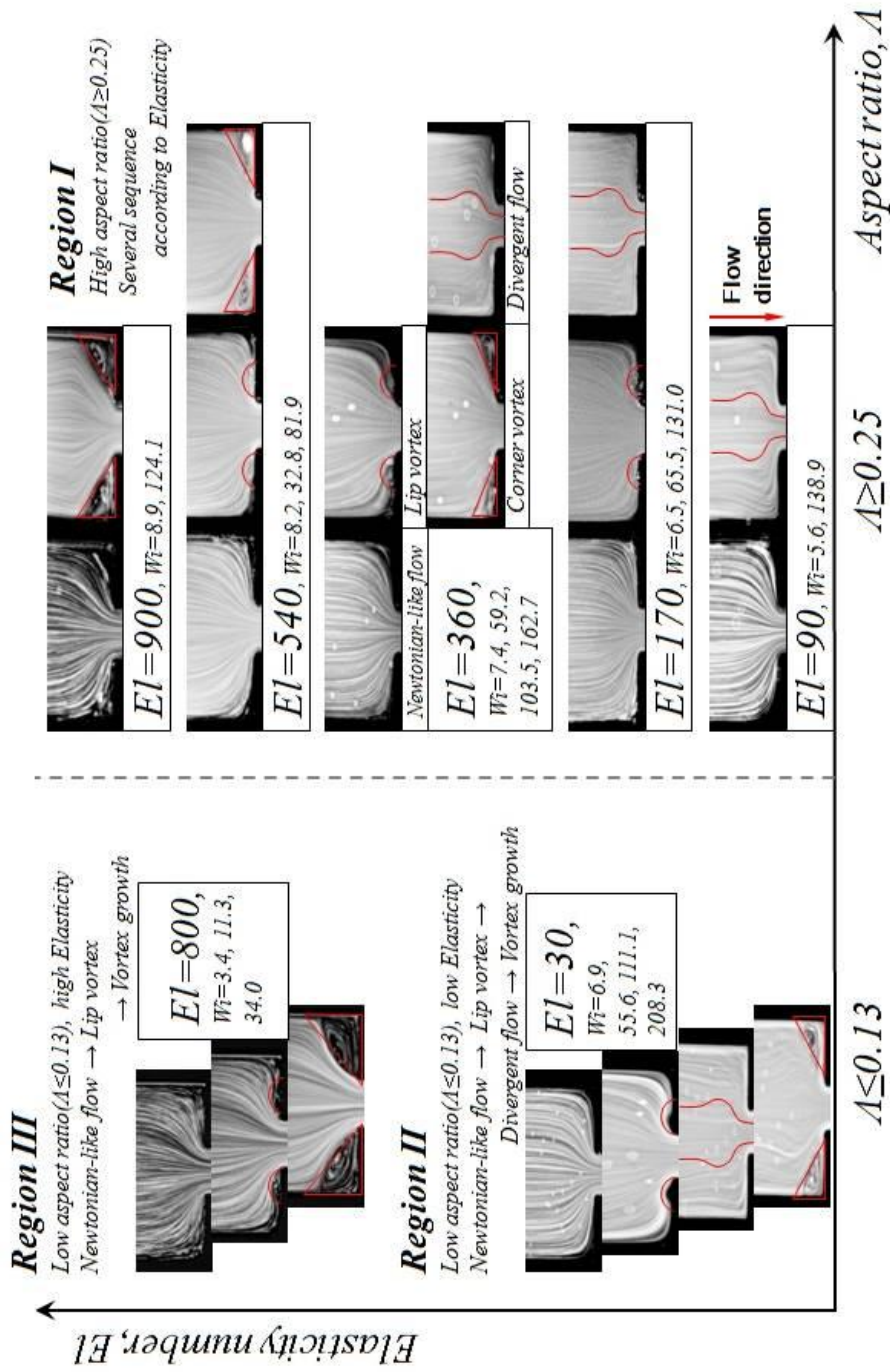
**Figure 3.6.** Map of the flow sequence with different aspect ratios and elasticity numbers. (Region I: Channel 3; Region II: Channel 4, $El$=30; Region III: Channel 5, $El$=800).

# 4. Time-Weissenberg number superposition

## 4.1. Method of experiment

The experiment was first performed by letting the three PEO solutions (2M 0.3wt% ($El$ =90), 0.7wt% ($El$ =1900), 1.0wt% ($El$ =5100)) in Figure 2.2. flow through Channel 3. In one set of experiments, the flow with a low $Wi$ was allowed to reach steady state, and the flow pattern at the steady state was recorded. The experiments were repeated as we increased $Wi$. This set of experiments was named as the steady set. In another set of experiments, the channel was first filled with fluid and the flow at the highest $Wi$ in the steady set was applied. The change inflow pattern was recorded until the flow fully developed and reached the steady state. This set of experiments was named as the transient set. The time when the highest flow rate was applied after filling the channel was defined as $t$ =0. After performing these two sets of experiments, the flow pattern from the first set (with the increase in $Wi$) and the flow pattern from the second set (with the increase in time) were compared, and those that had the same shape were matched. When these two sets were matched in the Newtonian-like flow region where there exists no particular flow pattern, it was hard to compare the steady set and transient set. The time at which the Newtonian-like flow ended was set to be $t_0$ and the graph was shifted by $t_0$. The time was non-dimensionalized by the relaxation time of the solution.

$$\tau = \frac{t - t_0}{\lambda}, \qquad - (4.1)$$

where $t$ is the elapsed time in the start-up flow; $t_0$ is the time at which the Newtonian-like flow ended; $\lambda$ is the relaxation time of the solution.

For the 0.3 wt% PEO solution, the steady state experiments were performed for $5.6 < Wi < 167$, and the transient flow experiment was performed at $Wi = 167$ from the time when the fluid began to flow ($t = 0$) to the time when the flow was fully developed ($\tau = 160$). For the 0.7 wt% PEO solution, the steady state experiments were performed for $33 < Wi < 550$, and the transient flow experiment at $Wi = 550$ for $\tau < 230$. The range of experiments is summarized in Table 4.1. The experiments were also performed using the same procedure with channel 4, 5, and 6 which are larger in size than the 200 μm: 50μm microchannel used above.

**Table 4.1.** Range of experiments in the steady and transient states in channel 3.

| | Steady ($Wi$) | Transient ($\tau$) |
|---|---|---|
| 0.3 wt% PEO | 5.6 - 167 | < 160 |
| 0.7 wt% PEO | 33 - 550 | < 230 |
| 1.0 wt% PEO | 14 - 690 | < 660 |

## 4.2. Results

When the channel geometry was changed, the flow pattern developed in different ways with the increase in $Wi$ or with the increase in time at a high $Wi$. For the 0.3 wt% and 0.7 wt% PEO solutions, there was no vortex with a low $Wi$ or an early-phase of a high $Wi$ flow in Channel 3. The flow was Newtonian-like, in which the streamlines were smooth as in a creeping flow with no flow separation. As elasticity increased, the divergent flow, in which the location of the maximum velocity was not right above the contraction entrance but more upstream, occurred and distorted the streamlines. Following the divergent flow, the vortex developed at the corners of the contraction zone. For the 0.3 wt% PEO solution in Channel 3, the flow was Newtonian-like for $Wi < 60$, a divergent flow for $60 < Wi < 120$, and a vortex growth for $Wi > 120$. When a high flow rate of $Wi = 170$ was applied, the flow was Newtonian-like for $\tau < 0$, a divergent flow for $0 < \tau < 50$, a vortex growth for $\tau > 50$, and finally reached the fully developed steady state at $\tau = 160$. The flow of the 0.7wt% solution was similar. It was Newtonian-like for $Wi < 300$, a divergent flow for $300 < Wi < 440$, and a vortex growth for $Wi > 440$. The flow was observed up to a $Wi$ of 550. For transient flow at $Wi$ of 550, the flow was Newtonian-like for $\tau < 0$, a divergent flow for $0 < \tau < 110$, and a vortex growth for $\tau > 110$. A fully developed steady state was reached at a $\tau$ of 230.

The steady flows of the 0.7wt% PEO solution with a low $Wi$ and the transient flows with a high $Wi$ were compared in Figure 4.2. In the divergent flow,
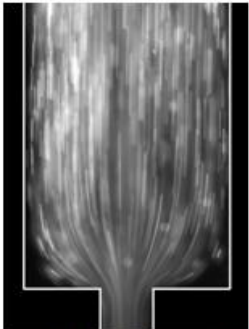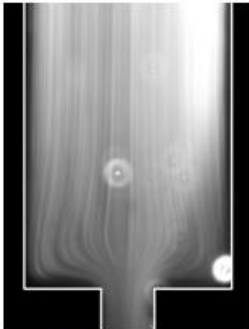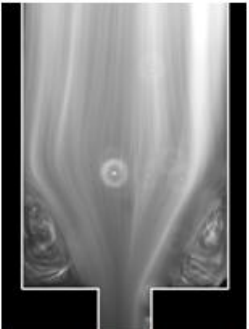
the distance between the two streamlines on both sides of the centerline decreased and then increased as the streamlines entered the contraction region. The narrow part is called the divergent throat and the wide part is called the divergent bulb. As the $Wi$ increased or as time passed with a high $Wi$, the divergent throat became narrower and the divergent bulb widened, leading to the change in the size ratio of these two.

When comparing the steady and transient states shown in Figure 4.2, the divergent flow region was compared using the ratio of the distance at the divergent throat and the distance at the divergent bulb between the two streamlines which were located at the same width with the contraction part. They are +25 μm and -25 μm from the centerline at the far upstream in channel 3. The steady flow with a $Wi$ of 380 and the transient flow after $\tau = 230$ with a $Wi$ of 550, shown in Figure 4.2, had a divergent throat of 138 μm wide and a divergent bulb of 176 μm wide. The ratio was 1.28. For the vortex growth, the size of the vortex increased as the $Wi$ increased or as time passed for the start-up flow with a high $Wi$. The vortex size was determined by measuring the length of the vortex in the flow direction at each corner along the channel side, and non-dimensionalized by upstream channel width. ($L_v / W_u$, $L_v$: vortex length, $W_u$: upstream channel width) The increase in the vortex size for the steady set and the transient set were also matched. When the $Wi$ was equal to 550, the vortex grew up to 0.5. A schematic of the size of the vortex shown in Figure 4.1.
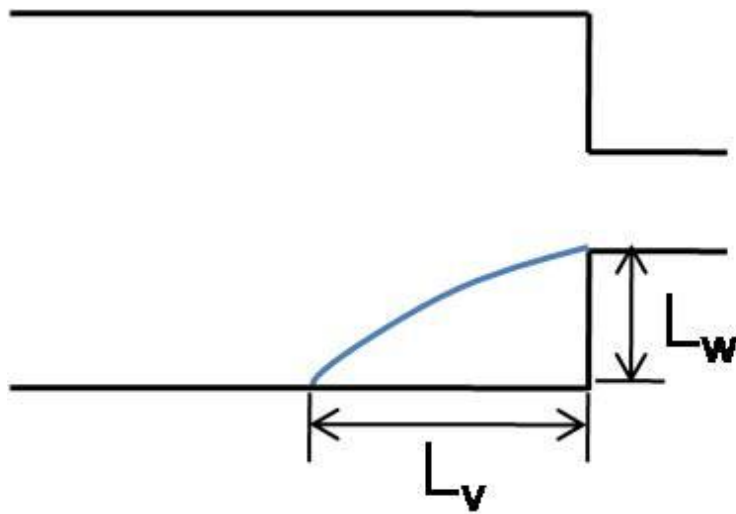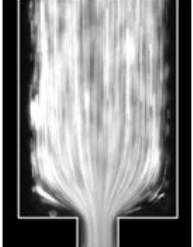
**Figure 4.1.** A schematic of the size of the vortex: $L_v$ is the maximum size of the oscillating vortex in the y direction and $L_w$ is the size of the vortex in the x direction.

|  | Newtonian-like | Divergent flow | Vortex growth |
|---|---|---|---|
| Steady | | | |
| | $Wi = 110, Re = 0.06$ | $Wi = 380, Re = 0.20$ | $Wi = 550, Re = 0.28$ |
| Transient | | | |
| | $\tau < 0$ | $\tau = 23$ | $\tau = 230$ |

**Figure 4.2.** Comparison of the steady flows with a low $Wi$ and transient flow with a high $Wi$ (=550) for 0.7 wt% PEO solution (2M).

The flow of the 1.0 wt% PEO solution was studied in the same manner, and the result is shown in Figure 4.3. However, as seen in the figure, the flow development in this case was different from the flow sequence of the 0.7 wt% solution. Asmentioned in previous section, the flow patterns in this region were diverse. For solutions with a concentration of 0.7 wt% or lower, the flow developed in the following sequence: Newtonian-like → divergent flow → vortex growth, and for the 1.0 wt% solution, a small corner vortex appeared shortly before the divergent flow in this experiment sets (weak vortex). The corner vortex that did not change in size and disappeared with a higher $Wi$ was named as the small vortex. As the $Wi$ increased or as time passed with a high $Wi$, the small corner vortices disappeared and the divergent flow occurred. For the divergent flow in this case, the ratio between the divergent bulb and the divergent throat was 1.31. When $Wi$ was 690, the dimensionless vortex size ($L_v/W_u$) was 0.5.

As seen in Table 4.2.(c), the flow was Newtonian-like for $Wi < 69$, a small vortex flow for $69 < Wi < 210$, a divergent flow for $210 < Wi < 410$, and a vortex growth for $Wi > 410$. The flow was observed until a $Wi$ of 690. For the transient case for a $Wi$ of 690, the same sequence as the low $Wi$ flows was reproduced. The flow was Newtonian-like for $\tau < 0$, a small vortex for $0 < \tau < 140$, a divergent flow for $140 < \tau < 290$, and a vortex growth for $\tau > 290$. The flow reached a fully developed steady state at $\tau = 660$.

| | Newtonian-like | Weak vortex | Divergent flow | Vortex growth |
|---|---|---|---|---|
| Steady | | | | |
| | $Wi = 41, Re = 0.008$ | $Wi = 140, Re = 0.03$ | $Wi = 280, Re = 0.05$ | $Wi = 690, Re = 0.14$ |
| Transient | | | | |
| | $\tau < 0$ | $\tau = 110$ | $\tau = 160$ | $\tau = 660$ |

**Figure 4.3.** Comparison of the steady flows with a low $Wi$ and transient flow with a high $Wi$ (=690) for 1.0 wt% PEO solution (2M).

**Table 4.2.** Flow sequence of the steady and transient flows. (a) Channel 3, 2M 0.3 wt% PEO, (b) channel 3, 2M 0.7 wt% PEO, (c) channel 3, 2M 1.0 wt% PEO, (d) channel 4, 2M 0.3 wt% PEO, (e) channel 5, 2M 0.7 wt% PEO, (f) channel 6, 2M 1.0 wt% PEO.

(a) Channel 3, 2M 0.3 wt% PEO

|  | Newtonian-like | Divergent flow | Vortex growth |
|---|---|---|---|
| Steady | $Wi < 60$ | $60 < Wi < 120$ | $Wi > 120$ |
| Transient | $\tau < 0$ | $0 < \tau < 50$ | $\tau > 50$ |

(b) Channel 3, 2M 0.7 wt% PEO

|  | Newtonian-like | Divergent flow | Vortex growth |
|---|---|---|---|
| Steady | $Wi < 300$ | $300 < Wi < 440$ | $Wi > 440$ |
| Transient | $\tau < 0$ | $0 < \tau < 110$ | $\tau > 110$ |

(c) Channel 3, 2M 1.0 wt% PEO

|  | Newtonian-like | Small vortex | Divergent flow | Vortex growth |
|---|---|---|---|---|
| Steady | $Wi < 69$ | $69 < Wi < 210$ | $210 < Wi < 410$ | $Wi > 410$ |
| Transient | $\tau < 0$ | $0 < \tau < 140$ | $140 < \tau < 290$ | $\tau > 290$ |

(d)Channel 4, 2M 0.3 wt% PEO

|  | Newtonian-like | Lip vortex | Divergent flow | Vortex growth |
|---|---|---|---|---|
| Steady | $Wi < 55$ | $55 < Wi < 100$ | $100 < Wi < 170$ | $Wi > 170$ |
| Transient | $\tau < 0$ | $0 < \tau < 30$ | $30 < \tau < 65$ | $\tau > 65$ |

(e) Channel 5, 2M 0.7 wt% PEO

|  | Newtonian-like | Lip vortex | Vortex growth |
|---|---|---|---|
| Steady | $Wi < 18$ | $18 < Wi < 40$ | $Wi > 40$ |
| Transient | $\tau < 0$ | $0 < \tau < 45$ | $\tau > 45$ |

(f) Channel 6, 2M 1.0 wt% PEO

|  | Newtonian-like | Lip vortex | Vortex growth |
|---|---|---|---|
| Steady | $Wi < 14$ | $14 < Wi < 45$ | $Wi > 45$ |
| Transient | $\tau < 0$ | $0 < \tau < 70$ | $\tau > 70$ |

Summarizing the results of the experiments performed with Channel 3, it can be seen that the flow patterns of the early-phase transient flow with a high $Wi$ matched well with the flow patterns of the steady states with a low $Wi$. The flow pattern developed in the same way when the $Wi$ increased for the steady flows and when time passed with a high $Wi$.

In order to check the universality of this observation, larger channels were also used. When channels larger than Channel 3 were used, a lip vortex was sometimes observed before the formation of the corner vortex instead of a divergent flow. However, as the $Wi$ increased, the corner vortex eventually appeared and kept on growing until the flow became unstable. The results with different polymer solutions and different flow channels are all summarized in Table 4.2. In this case, a device time-scale that is caused by the compressibility of the fluid or device may be existed. Difference in time-scale among the channels was characterized by pressure drop measurement. Pressure tips were set on the contraction part of the channel, and the channel and the tube were filled with DI water or PEO solutions. However, even with channel 6, the biggest, the total pressure drop increased immediately after running the syringe pump. Therefore, the time scale of the device was not significant.

## 4.3. Time-Weissenberg number superposition

When the patterns of the two sets of experiments were matched between the steady flow with a low $Wi$ and transient flow with a high $Wi$, we marked a point on

the graph in Figure 4.4, where the x-axis is the $\tau$ in the transient set and the y-axis is the $Wi$ in the steady set. As various channel geometries and solutions were used, the range of $Wi$ was large and the y axis was represented in log scale. Through this graph, the relationship between the flow patterns of the two sets of experiments in the process of flow development could be examined.

As seen in Figure 4.3, all the curves followed a similar form regardless of the channel size and fluids. The change in flow patterns was the different for different flow conditions, but the slope of the curve changed significantly at the point where the corner vortex first appeared. It is similar to numerical results of Szabo et al. in a way that the slope of the pressure drop versus time significantly decreased when the motion of vortex center changed. (Szabo et al. 1997) More important is that we could plot the curve for all the experiments we performed, which means that there always exists a relationship between the time and $Wi$, or between the steady flow patterns with a low $Wi$ and the transient flow patterns with a high $Wi$. From this, it can be suggested that there exists a relationship between time and $Wi$ in vortex dynamics, which could be named as the time-Weissenberg number superposition.
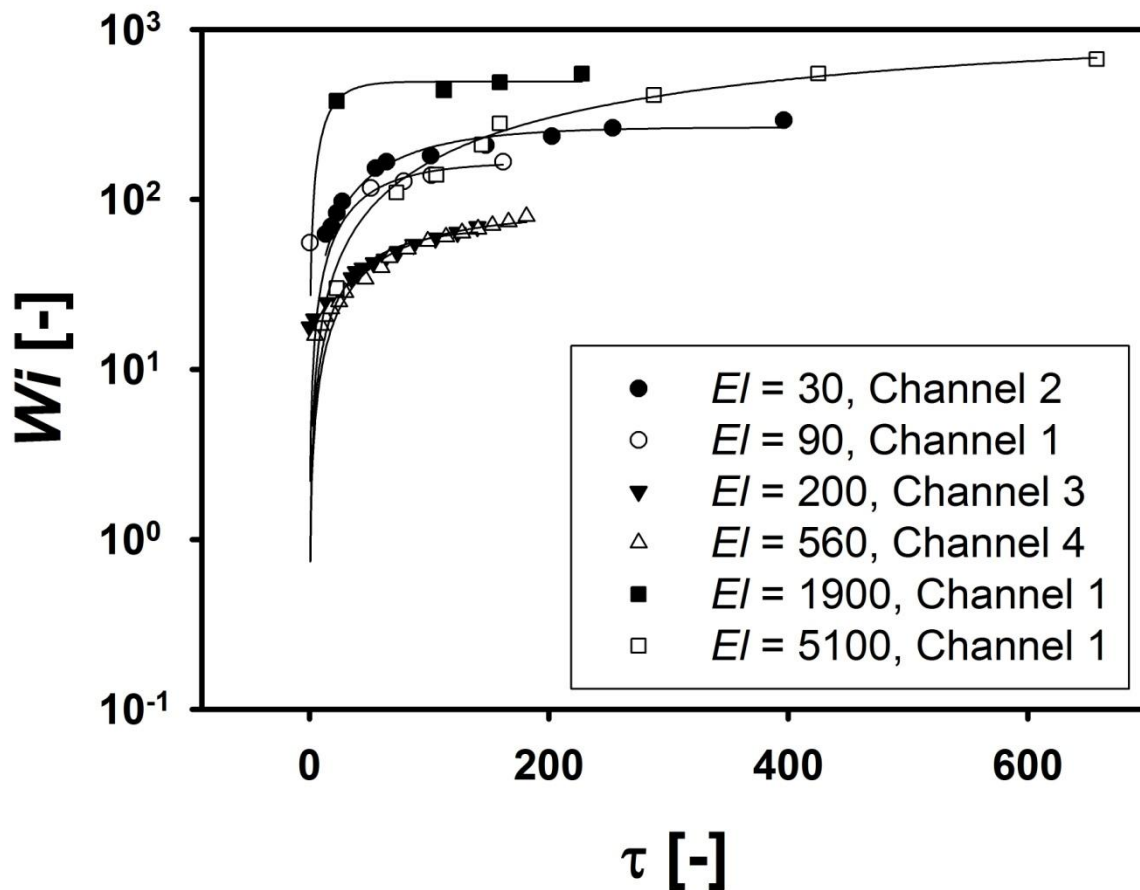
**Figure 4.4.** Time-*Wi* superposition graphs. 1) *El* = 30, 2M PEO 0.3 wt% Channel 4, 2) *El* = 90, 2M PEO 0.3 wt% Channel 4, 3) *El* = 200, 2M PEO 0.7 wt% Channel 5, 4) *El* = 560, 2M PEO 1.0 wt% Channel 6, 5) *El* = 1900, 2M 0PEO 0.7 wt% Channel 3, 6) *El* = 5100, 2M PEO 1.0 wt% Channel 3.

In the 2-D simulation of the 4:1 planar contraction flow with the Oldroyd-B model, the time-$Wi$ superposition was also confirmed. In the simulation, both the lip vortex and the corner vortex were observed and they grew as the $Wi$ increased or as time passed for the start-up with a high $Wi$ flow. Eventually, the two vortices coalesced, forming a big corner vortex. The slope changed significantly at the point where the lip and corner vortex coalesced. (Kim et al. 2005) The experiments show different flow sequences compared to the simulation. Unlike the simulation in which both the lip and corner vortex formed and coalesced, the flow developed to the divergent flow, which was not observed in the 2-D simulation, and either the corner vortex or lip vortex eventually grew in size to reach the corner of the microchannel. Although the process to form a large corner vortex was slightly different compared to the simulation, the one-to-one matching of the flow patterns between the transient and steady flows was the same, and the slope in the time-$Wi$ graph decreased significantly at the point of the vortex formation for both cases. As seen from the experimental results with the various fluids, if a certain flow pattern appears in the steady state with a low $Wi$, such a flow pattern will appear in the early-phase of the transient flow with a high $Wi$, and vice versa.

The time-$Wi$ superposition was demonstrated experimentally as shown in Figure 4.3. Even though different fluids and different channels were used, all the curves followed a similar form that could be fitted into the equation, $Wi = a(1 - e^{-b\tau})$. Each point in the figure represents the results of two sets of experiments (steady and transient), and the lines are the fitted results using the equation above. Table 4.3 lists

the fitting parameters. The physical meaning of the parameters is yet unclear and more research will be necessary. However, despite the fact that different fluids and different channels were used, the time and $Wi$ had a special relationship that could be represented by a single curve. From this, it could be concluded that the vortex dynamics of viscoelastic fluids in the contraction flow could be dominated by a simple rule, which is the time-$Wi$ superposition.

**Table 4.3.** Fitting parameters of each time-$Wi$ superposition graph, following the equation $Wi = a(1-e^{-b\tau})$.

| Channel | $El$ | a | b |
|---|---|---|---|
| Channel 2 | 30 | $2.66 \times e^2$ | $1.42 \times e^{-2}$ |
| Channel 1 | 90 | $1.65 \times e^2$ | $2.13 \times e^{-2}$ |
| Channel 3 | 200 | $6.83 \times e^1$ | $1.99 \times e^{-2}$ |
| Channel 4 | 560 | $8.11 \times e^1$ | $1.30 \times e^{-2}$ |
| Channel 1 | 1900 | $4.94 \times e^2$ | $6.39 \times e^{-2}$ |
| Channel 1 | 5100 | $9.56 \times e^2$ | $1.90 \times e^{-3}$ |

# 5. Unstable flows

## 5.1. Sequence of developing flow pattern of highly elastic fluids

In this section, to observe unstable flows, usually 5,000,000 molecular weight polyethylene oxide solutions in Figure 2.2 were used, and only one channel geometry (channel 3, 200μm:50μm) was used. Figure 5.1 shows the sequence of developing flow patterns as as the *El* or *Wi* increased in this condition. The flow was Newtonian-like at first where the fluid enters the contraction smoothly without any unusual flow pattern (Newtonian fluids do not exhibit any unusual flow patterns inside a microchannel). From the Newtonian-like flow (A), a corner or lip vortex (B) was formed as the elasticity increased. Because (B) disappears as the flow rate is increased further, it is called a weak vortex. As the weak vortex disappeared, a divergent flow (C) was observed, in which the maximum velocity was not at the contraction but in the upstream region. (Rodd et al. 2007; Alves & Poole 2007) As the elasticity increased further, a vortex growth region (D) was observed, in which the size of the steady vortex increased with *Wi*. When the elasticity was increased further, the flow transitioned from the steady to the unsteady region, and exhibited continuous fluctuations. In this region, the vortex fluctuated with a certain period instead of maintaining a steady vortex. This was called oscillating vortex (E). After that, vortex fluctuation lost its periodicity, and aperiodic fluctuation regime appeared (F).

**(A)** Newtonian-like

**(B)** Weak vortex

**(C)** Divergent

**(D)** Vortex growth

**(E)** Oscillating vortex

**(F)** Aperiodic fluctuation
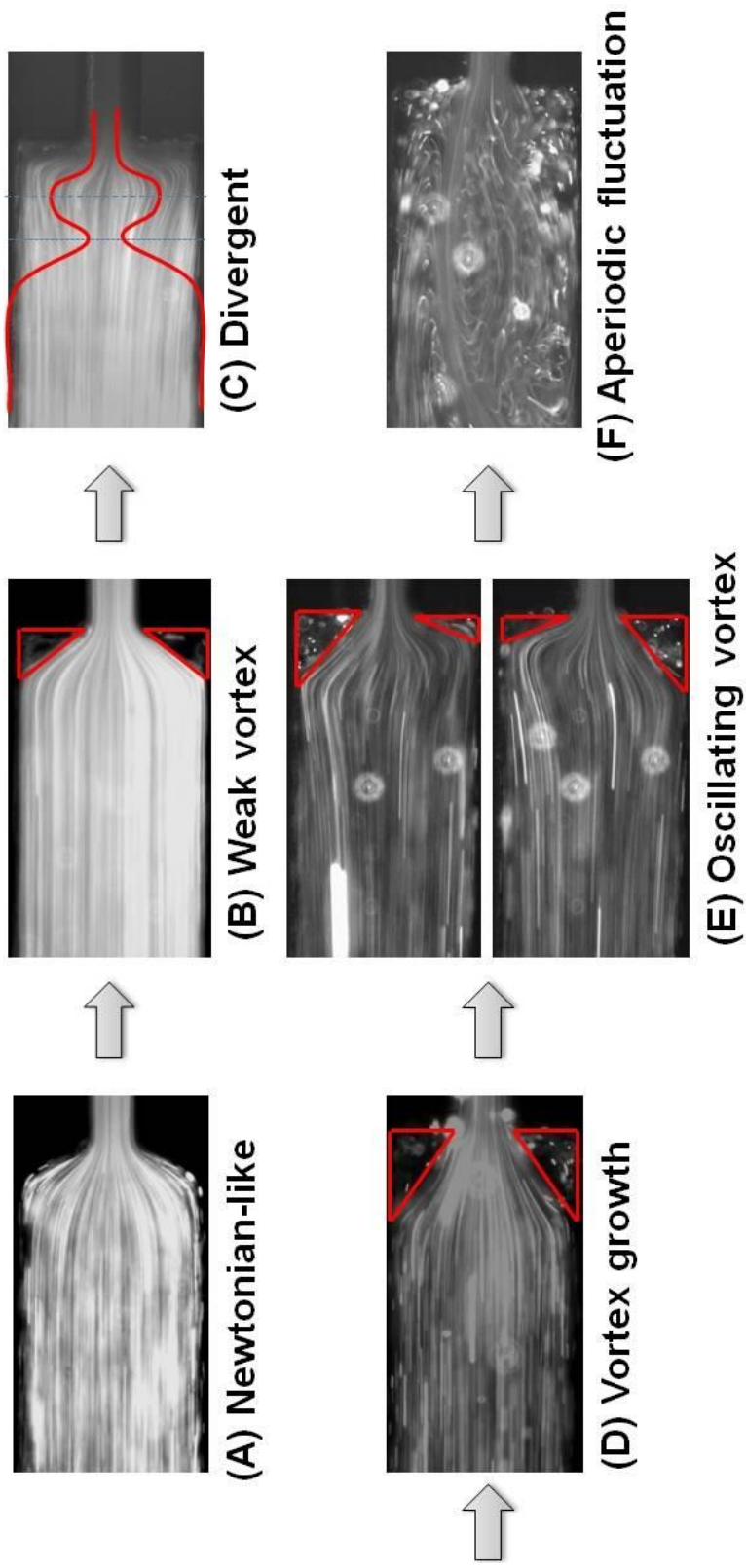
**Figure 5.1.** The sequence of developing flow patterns with increasing elasticity of fluids and the shear rate of the flow.

The sequence was identified by mapping the flow patterns as shown in Figure 5.2. The change in the flow pattern from A to F indicates the change with the increase in $Wi$, while the change in flow patterns from the left to the right side of the table indicates the change with the increase in $El$. The flow patterns were influenced by both $Wi$ and $El$. (Rodd et al. 2007) For dilute polymer solutions with low $El$, it was difficult to reach the steady vortex region because the shear rate was limited by a maximum pressure that the micro-fabricated PDMS channel can endure. The maximum flow rate was dependent on the viscosity of the solution. The viscosity range of the solutions, in this section, was $0.17 < \eta_0 < 39$ Pa s. The maximum $Q$ was 15 ml/hr for $\eta_0 = 0.17$ Pa s, and 2 ml/hr for $\eta_0 = 39$ Pa s.

Due to the limitation of the shear rate, solutions with high concentrations and high molecular weight were used to observe the flow change at low shear rates. Unlike the case with the dilute polymer solutions, an unusual flow pattern with a vortex was observed even at low shear rates with these solutions. And it was difficult to observe the Newtonian-like flow pattern that was observed for the dilute solutions. As can be seen in Figure 5.2, a weak vortex was observed for 0.4 wt% 5M PEO solution even at the lowest flow rate allowed by the syringe pump resolution (approximately 0.05ml/hr). For a 0.7 wt% 5M PEO solution, a vortex growth region was observed at this flow rate. In these cases, even though a Newtonian-like flow or a divergent flow could not be observed, the oscillating vortex and aperiodic fluctuation could be observed.
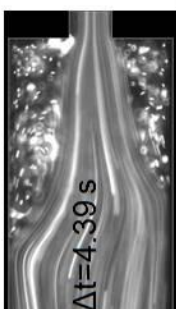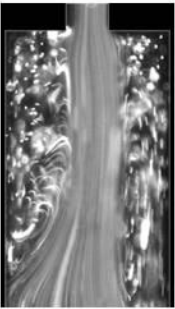
**Figure 5.2.** The map of the sequences in the flow development with various solutions containing 1.0 wt% ($M_w$=2 × 10$^6$ g mol$^{-1}$), 0.4 wt%, 0.7 wt%, and 1.0 wt% ($M_w$ =5 × 10$^6$ g mol$^{-1}$) PEO.

## 5.2. Oscillating vortex

As the elasticity or shear rate increased, the flow transitioned from a steady vortex to an oscillating vortex where the vortex fluctuated with a period. The flow pattern is shown in Figure 5.3. The oscillating vortex could be categorized as symmetric and asymmetric according to its pattern of vortex formation. In the symmetric oscillating vortex, the maximum and minimum sizes of the corner vortex at one corner of the channel were the same with those at the other corner. When one corner vortex was at its minimum, the other was at its maximum size. However, in the asymmetric oscillating vortex, the maximum size and the minimum size of the two corner vortices, or the periods of two vortices were not the same. In other words, symmetric oscillating vortex is equivalently alternating, and asymmetric oscillating vortex is inequivalently alternating.

(a)

| Wi | Period | Type | Vortex transition | | |
|---|---|---|---|---|---|
| 81 | 5.10 s | Symmetric | | Δt=2.55 s | Δt=5.10 s |
| 98 | 5.75 s | Asymmetric | | Δt=2.70 s | Δt=5.75 s |
| 114 | 5.60 s | Asymmetric | | Δt = 2.92 s | Δt = 5.60 s |

(b)

**Figure 5.3.** Vortex transition features of the oscillating vortex for (a) 0.7 wt% 5M PEO solution (b) 0.8 wt% 5M PEO solution (c) 1.0 wt% 5M PEO solution.

Figure 5.3 shows the oscillating vortices for 3 different solutions of 0.7 wt%, 0.8 wt%, and 1.0 wt% 5M PEO. The fluids were highly elastic with an $El$ range of 2.7 X $10^6$< $El$ <2.2 X $10^6$. The flow rate was 0.2< $Q$ <1.0 ml/hr and the Weissenberg number ranged from 50< $Wi$ <130. The experiments were not completely reproducible because the flow was in an unstable region with high elasticity, and aperiodic vortex fluctuation was often observed even at a $Wi$ slightly higher than the $Wi$ region where oscillating vortices were observed. Therefore, the experiments were repeated until reproducible results were obtained. For the 0.7 wt% solution, a symmetric oscillating vortex was easily observed. But as the concentration increased, the asymmetric vortex was observed. For a 1.0 wt% solution, the symmetric oscillating vortex was not observed in the controllable volumetric flow rate even though the experiments were repeated many times. From these results, it can be deduced that the oscillating vortex had a tendency to transit from a symmetric to asymmetric flow with an increase in $El$ or $Wi$.

In the oscillating vortex region, the vortex fluctuated with a certain period as described above. In the 200 μm:50 μm channel system used in this study, the period was in the range of 2<period<6 s shown in Figure 5.4. This was nearly a hundred times larger than the characteristic time of the flow (the time to pass through the upstream channel with an average velocity ($\frac{Q}{W_u \times h}$)) or the characteristic time of the fluids ($\lambda$). The results with the 5M PEO solutions with 0.6< $C$ <1.0 wt% are given in the figure, with the x-axis as $Wi$ and y-axis as the period. As can be seen in the graph, all the results were within the range, but no functional relationship could be found

because it was in the unstable region, and the flow was right before losing its periodicity.

The vortex size increased with the increase in $Wi$ in the vortex growth region. Because the vortex size changed constantly in the oscillating vortex region unlike the steady region, the maximum size of the vortex was measured in Figure 5.5 during fluctuation. The results are for 5M PEO solutions with the concentration in the range of $0.6 < C < 1.0$ wt%. As can be seen in the schematic of Figure 4.1, $L_v$ is the maximum size of the oscillating vortex in the y-direction (flow direction) and $L_w$ is the size of the vortex in the x-direction. $L_w$ was fixed at 75μm. In Figure 5.5, the x-axis represents $Wi$, and the y-axis represents the dimensionless vortex size ($L_v / L_w$). In the oscillating vortex region, though the vortex size changed continuously, the maximum vortex size increased with $Wi$.

To quantitatively analyze the pattern of the oscillating vortex, the vortex size at each corner of the channel was measured over time and the results are graphed in Fiure 5.6. $L(i)$ represents the size of the vortex on the left hand side of the flow direction and $R(i)$ is that on the right hand side. Figure 5.6 (a) is the result for the 0.7 wt% 5M PEO solution with a $Wi$ of 79 and $Q$ of 0.5 ml/hr. The oscillating vortex fluctuated symmetrically, with the vortex at each side having the same maximum and minimum vortex size with the same period. When the size of the vortex was plotted over time, a periodic curve could be drawn. The change in size of two vortices was alternated by half of a period. In addition, whether the oscillating vortex was symmetric or asymmetric, the vortex size did not decrease immediately after reaching
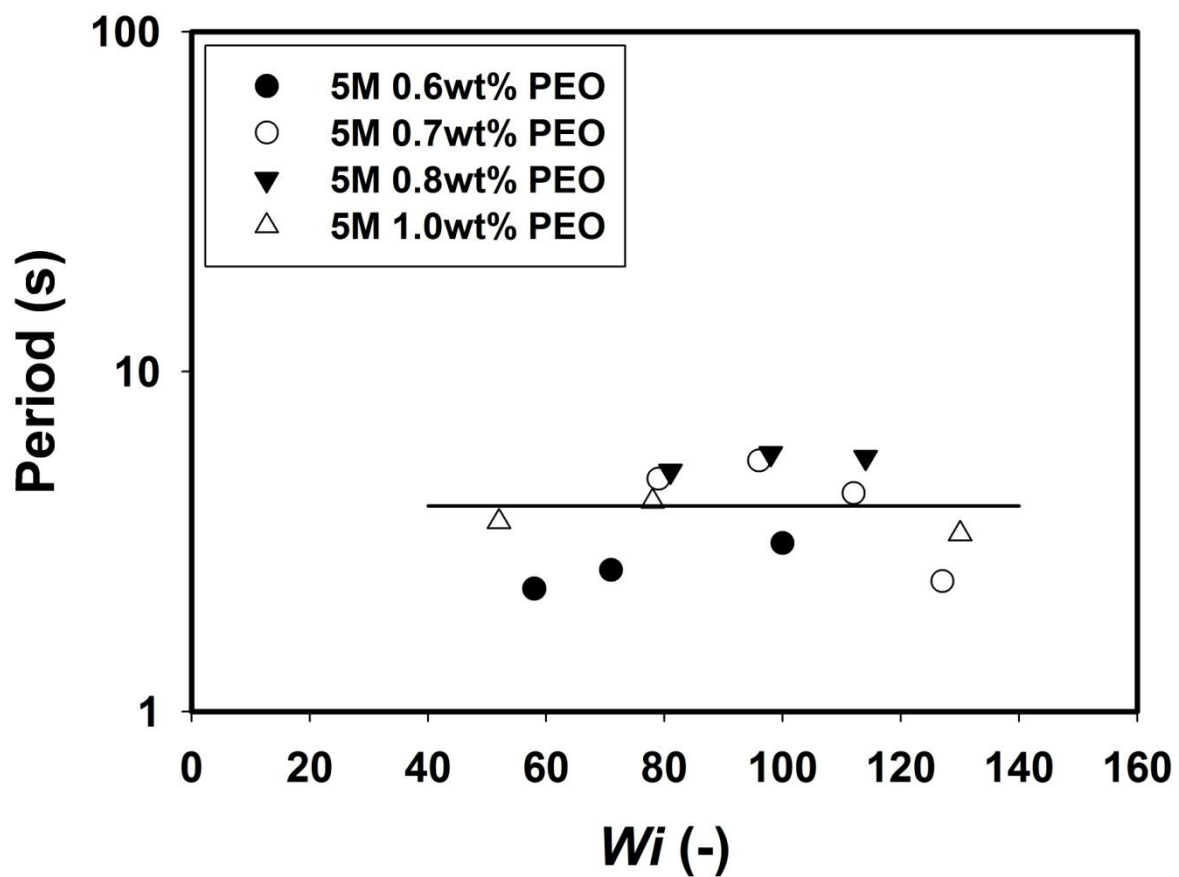
**Figure 5.4.** Periods of the oscillating vortex for 0.6, 0.7, 0.8 and 1.0 wt% PEO solutions ($M_w$=5×10$^6$ g mol$^{-1}$) in a wide range of Weissenberg numbers. (The line in graph is a simple guideline.)
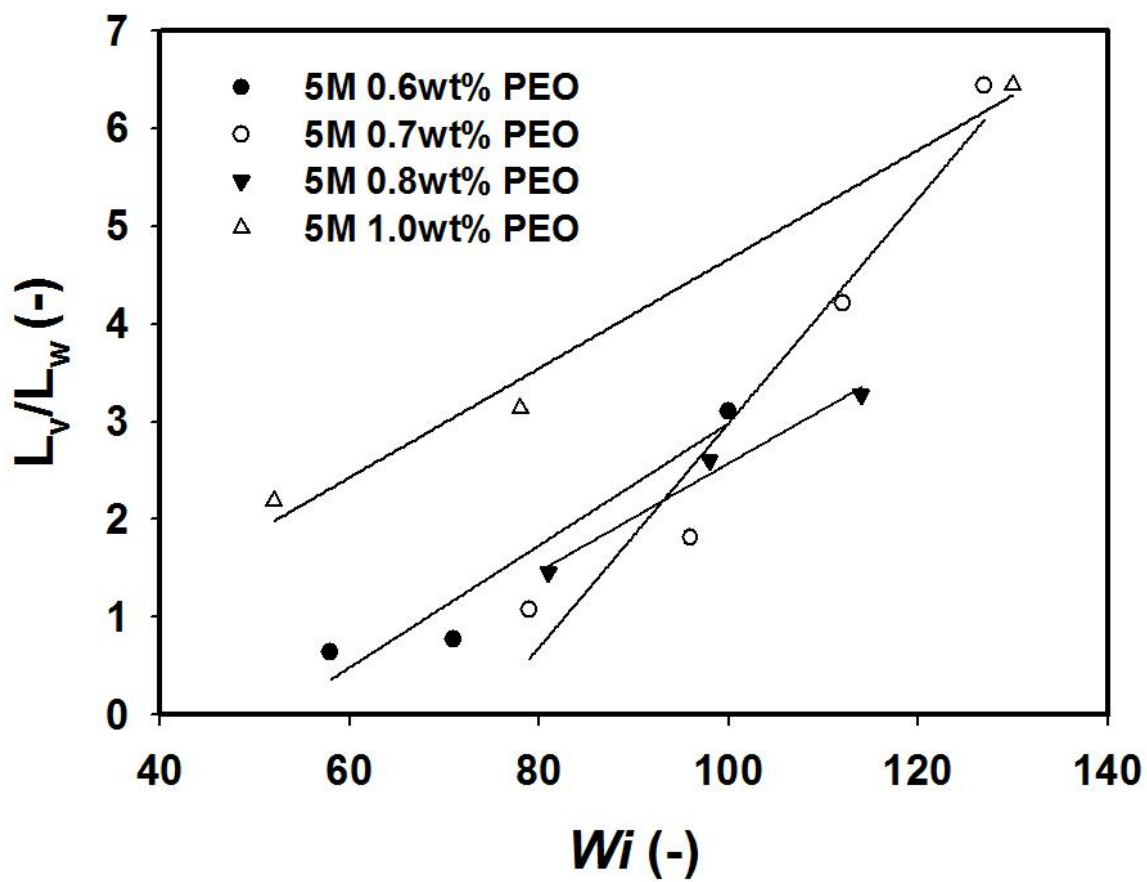
**Figure 5.5.** Maximum size of the oscillating vortex for 0.6, 0.7, 0.8 and 1.0 wt% PEO

solutions ($M_w$ =5×10$^6$ g mol$^{-1}$)

its maximum. The vortex maintained its maximum size for a few seconds before shrinking.

Although the symmetric oscillating vortex exhibited only one type of size change as can be seen in Figure 5.6 (a), the asymmetric oscillating vortex exhibited different patterns. They could be categorized into two patterns shown in Figure 5.6 (b) and (c). In one case, one vortex fluctuated significantly while the other rarely fluctuated shown in (b). In another, shown in (c), the two vortices fluctuated with different patterns but with a single period. For example, in Figure 5.6 (c), the left vortex maintained its maximum for 2 seconds and decreased to its minimum size of 30 μm while the right vortex stayed at the maximum for 1.2 seconds and decreased to its minimum size of over 50 μm. The asymmetric oscillating vortex showed irregularities compared to the symmetric oscillating vortex, but still repeated irregular flows with a constant period.
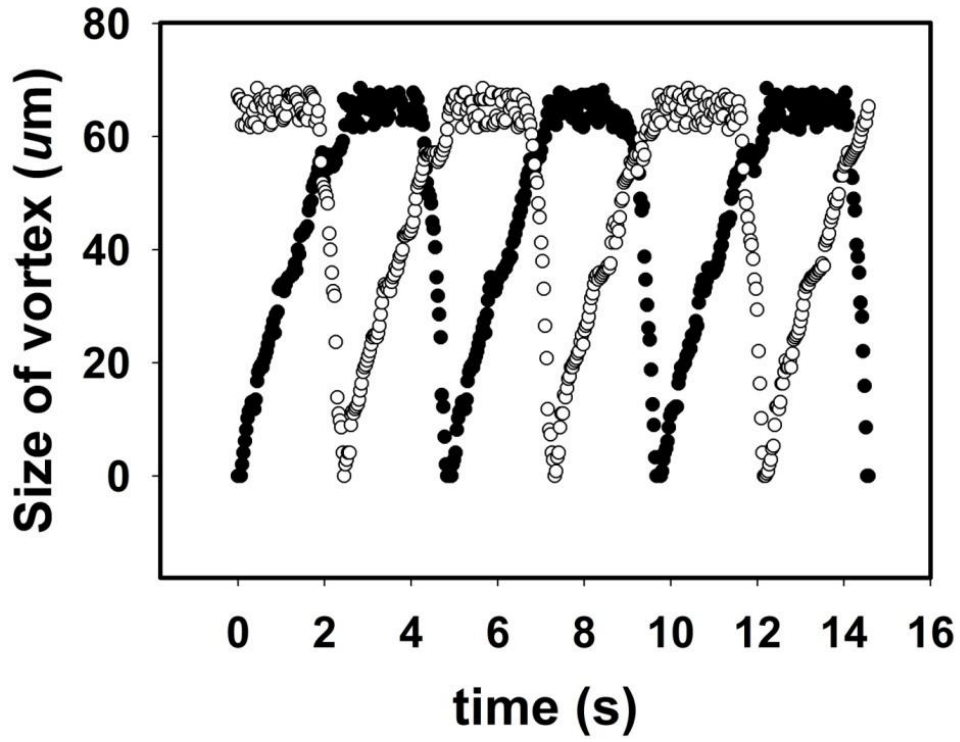
(a)
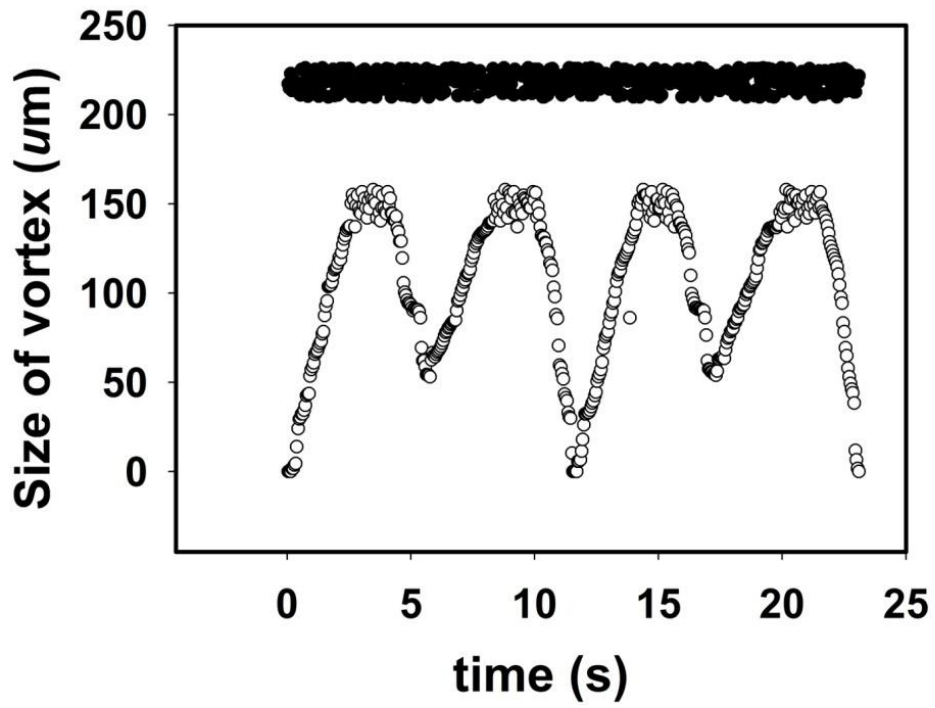


(b)
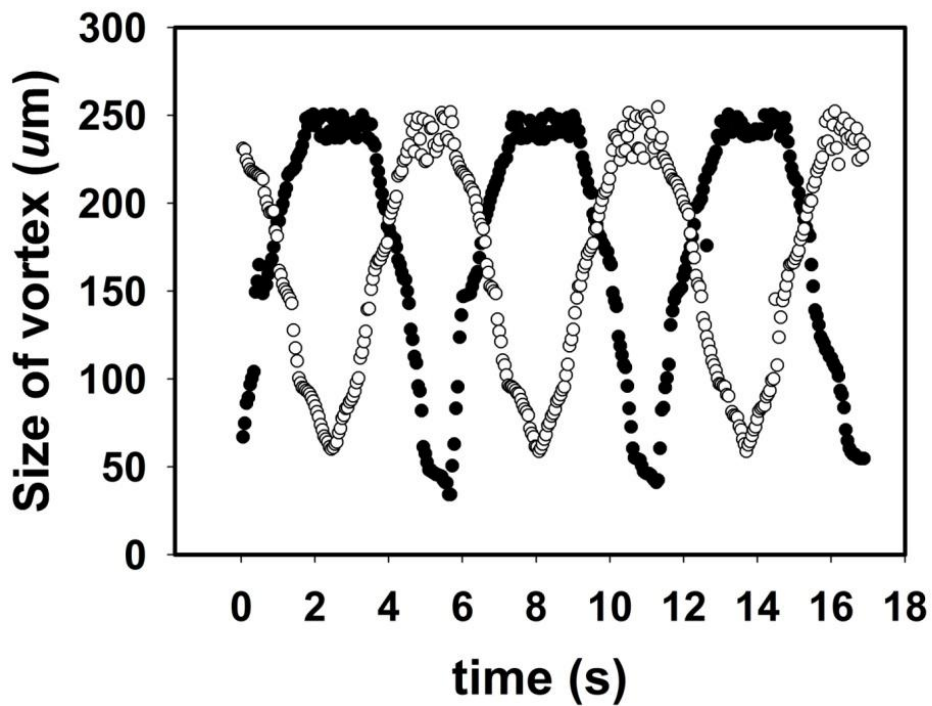
(c)

**Figure 5.6.** The patterns of the oscillating vortex with sizing by time (a) Symmetric ($El = 2.7 \times 10^5$, $Wi = 79$): changes in vortex size for $L(i)$ is the reverse of $R(i)$. (b) Asymmetric 1 ($El = 2.9 \times 10^5$, $Wi = 98$): $L(i)$ is fixed and $R(i)$ is oscillating. (c) Asymmetric 2 ($El = 2.9 \times 10^5$, $Wi = 114$): oscillating patterns of $L(i)$ and $R(i)$ are different in a period. ($\bullet$: $L(i)$, $\circ$: $R(i)$ for each graph)

## 5.3. Aperiodic fluctuation

When *Wi* increased further after the oscillating vortex, the aperiodic fluctuation regime in which the vortex fluctuated randomly without a characteristic time scale appeared. The vortex at each side changed very rapidly without a pattern. Sometimes, the two vortices overlapped. When the size of the oscillating vortex was measured over time and plotted, a specific time periodicity appeared seen in Figure 5.6. However, when the vortex size was plotted in this region, no apparent period could be observed as shown in Figure 5.7, which shows the vortex size of the left and right sides versus time for 5M PEO 0.7 wt% solution at $El = 2.2 \times 10^6$ and *Wi* $= 2.8 \times 10^2$.

In order to check whether the flow in this region was chaotic, the largest Lyapunov exponent was calculated. (Sprott 2003; Rosenstein et al. 1993) In a 2D graph, if there exists anarbitrary point $X = X^*$ and $Y = Y^*$ that satisfies

$$\frac{\partial X}{\partial t} = F(X, Y) \qquad\qquad - (5.1)$$

and

$$\frac{\partial Y}{\partial t} = G(X, Y), \qquad\qquad - (5.2)$$

the transients of $X$ and $Y$ are

$$\frac{\partial X}{\partial t} = \Delta X \left.\frac{\partial F}{\partial X}\right|_{(X^*, Y^*)} + \Delta Y \left.\frac{\partial F}{\partial Y}\right|_{(X^*, Y^*)} \qquad - (5.3)$$

and

$$\frac{\partial Y}{\partial t} = \Delta X \left.\frac{\partial G}{\partial X}\right|_{(X^*,Y^*)} + \Delta Y \left.\frac{\partial G}{\partial Y}\right|_{(X^*,Y^*)} \qquad \text{- (5.4)}$$

at the point $X = X^* + \Delta X$ and $Y = Y^* + \Delta Y$ which are very small distance away from the point $X = X^*$ and $Y = Y^*$. Then, there exists the following relation:

$$\begin{pmatrix} \left.\dfrac{\partial F}{\partial X}\right|_{(X^*,Y^*)} & \left.\dfrac{\partial F}{\partial Y}\right|_{(X^*,Y^*)} \\ \left.\dfrac{\partial G}{\partial X}\right|_{(X^*,Y^*)} & \left.\dfrac{\partial G}{\partial Y}\right|_{(X^*,Y^*)} \end{pmatrix} \begin{pmatrix} \Delta X \\ \Delta Y \end{pmatrix} = \begin{pmatrix} \dfrac{\partial X}{\partial t} \\ \dfrac{\partial Y}{\partial t} \end{pmatrix}. \qquad \text{- (5.5)}$$

From the eigenvalue $\lambda$ of the above equation, the behavior of the position with respect to an infinitesimally small change in location can be determined. If the eigenvalue is positive, the infinitesimally small change is amplified over time while it decreases over time when the eigenvalue is negative. The eigenvalues are defined only at a specific point where $X = X^*$ and $Y = Y^*$. The Lyapunov exponent is the average of the eigenvalues for every point that exists over a long time. The number of Lyapunov exponents is equal to the number of dynamic variables of the system. The largest Lyapunov exponent signifies how a point that is a certain distance away from another point gets close or moves away. The largest positive Lyapunov exponent implies that the change is amplified over time when the system variables are changed by a small amount. This can be defined as chaotic.

The largest Lyapunov exponents for the vortex size of both left and right hand side were determined from the data in Figure 5.7. For each vortex, one thousand data points were analyzed. For the multiple points with $j$ amount of pairs, the pair with the least distance between the points was selected. The distance between the points of
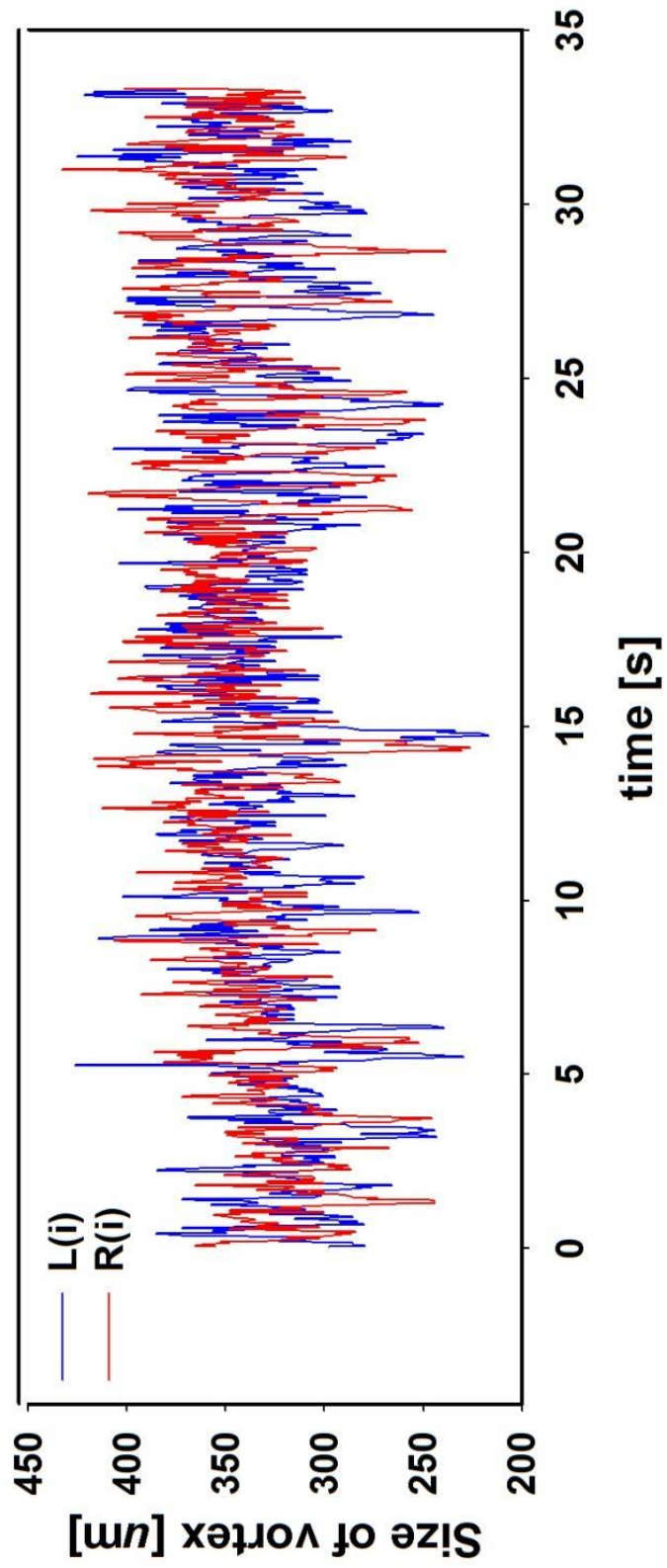
**Figure 5.7.** Size of the vortex in the aperiodic fluctuation regime for the flow of $El = 2.2 \times 10^6$ and $Wi = 2.8 \times 10^2$.

this pair after a certain amount of time was defined as $d_j(i)$ where $i$ is the discrete-time step, and this is the divergence. $\Delta t$ is the sampling period, which is 1/30 second in this experiment. In other words, the time after $i$ steps is $i\Delta t$. According to Rosenstein et al., when the largest Lyapunov exponent is $\lambda_1$, the relationship of $d_j(i) \approx C_j e^{\lambda_1(i\Delta t)}$ can be defined, where $C_j$ is the initial distance between the pair of two points that are closest to each other among the $j$ pairs. Taking the logarithm of this equation, $\ln d_j(i) \approx \ln C_j + \lambda_1(i\Delta t)$ can be derived. The average of $j$ number of pairs could be plotted in Figure 5.8 for both left and right side of vortex. The x-axis is $i\Delta t$ (time) and y-axis is the average of $\ln d_j(i)$ with its slope being $\lambda_1$, the largest Lyapunov exponent. As shown in Figure 5.8, it initially increases rapidly with the slope of approximately ten. When the largest Lyapunov exponent is positive as in this case, the dynamics, the motion of vortex in this case, can be considered be chaotic.

Power spectra of the vortex size at $Wi = 2.8 \times 10^2$ is given in Figure 5.9. The large peak in small frequency less than 0.1 is irrelevant to the actual vortex fluctuation. There is no any characteristic peak, which also supports the flow is chaotic in this region.

Newtonian fluids did not exhibit distinctive flow patterns such as vortex formation in micro-contraction channel flow. For viscoelastic fluids, the nonlinear rheological characteristics caused various flow patterns even at very low Reynolds numbers. The present work analyzed the overall flow patterns in the contraction geometry, especially unsteady region with micro-scale devices. In unsteady flows regime, the oscillating vortex lost its periodicity at high $Wi$. It is similar to such

elasticity-induced turbulence which was observed in various flows such as in the simple shear flow between the parallel plates, Couette-Taylor flow between the two cylinders, and the curvilinear channel flows. (Groisman & Steinberg 2000; Groisman & Steinberg 2004; Fardin et al. 2010)
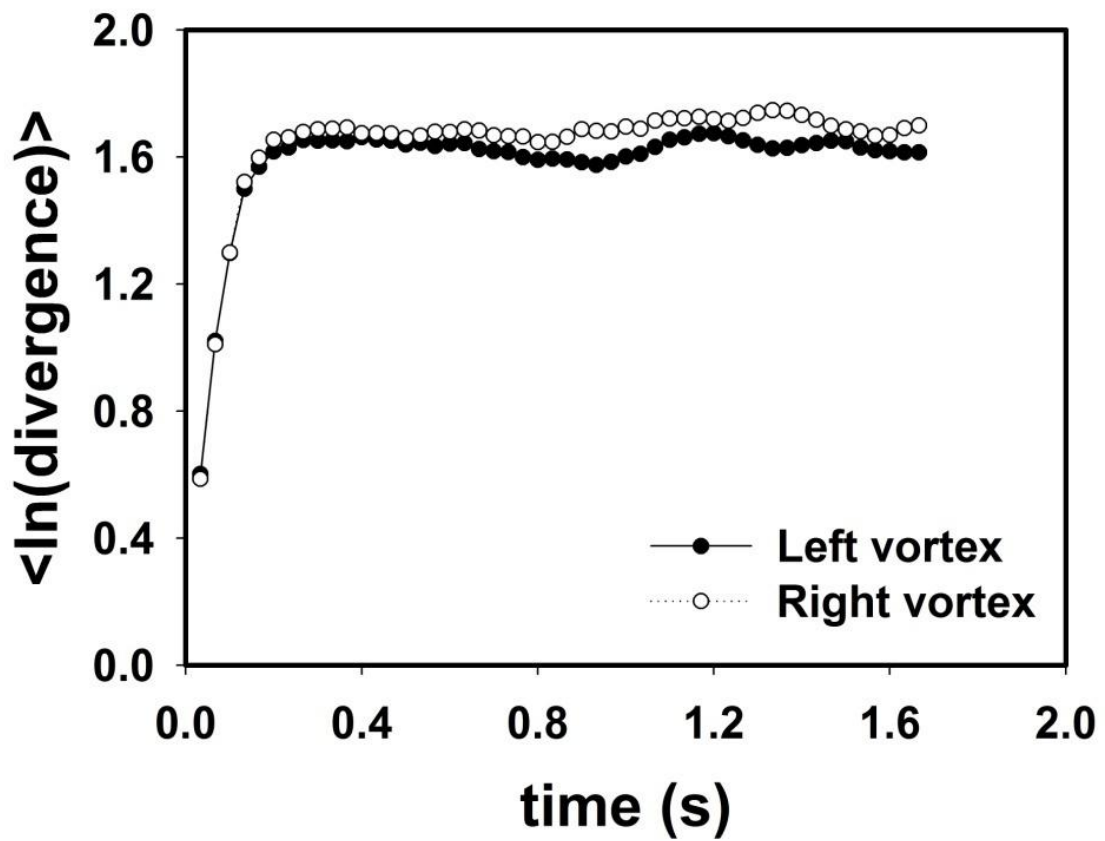
**Figure 5.8.** Plot of <ln(divergence)> vs. time for the vortex size of the aperiodic fluctuation. ($\bullet$: $L(i)$, $\circ$: $R(i)$ for each plot)
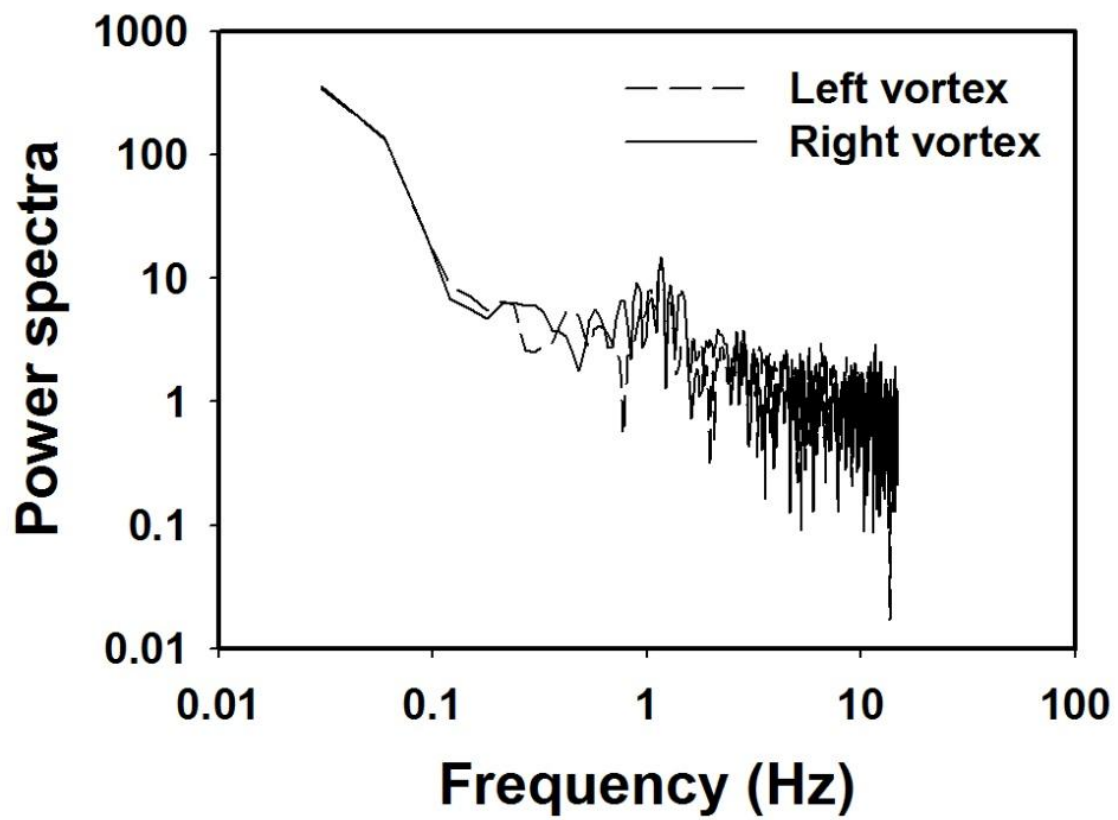
**Figure 5.9.** Power spectra of change of vortex size in the aperiodic fluctuation regime. ( $El = 2.2 \times 10^6$ and $Wi = 2.8 \times 10^2$ )

# 6. Summary

## Dynamics of flow in contraction geometry

First, the flow dynamics of viscoelastic fluids inside 4:1 planar micro-contraction channels was investigated. The flow showed various flow patterns caused by elasticity. From the observation of the flow sequence over a wide range of Weissenberg number ($Wi$) and elasticity number ($El$), the viscoelastic flow developed starting from a Newtonian-like flow to a flow with a lip vortex region in which small vortices near the contraction part appeared. The lip vortex grew into a corner vortex. The corner vortex then disappeared and a divergent flow, in which the maximum velocity occurred not at the contraction part but further upstream with distorted streamlines, was formed. Finally, as the $Wi$ was increased further, the corner vortex formed again, and the flow reached the vortex growth region where the size of the vortex continued to increase with the increase in $Wi$. Although the sequence of the flow development never changed, certain phases of the flow development were omitted according to the flow conditions. The primary factors affecting the flow sequence were the aspect ratio of the channel and the elasticity number. Using multiple channels with different sizes and PEO solutions with varying concentrations, the effect of the channel aspect ratio and $El$ was analyzed. In the case of a low aspect ratio, the lip vortex always appeared, and the divergent flow occurred only when $El$ was low. When the aspect ratio of the channel was higher, the flow pattern

prior to the vortex growth region was more diverse. In the case of a high aspect ratio channel, the flow patterns between Newtonian-like flow and vortex growth region were diverse. The critical aspect ratio at which the transition from a low aspect ratio flow to a high aspect ratio flow occurred was between 0.13 and 0.25 for the 70 μm height channels.

**Time-*Wi* superposition**

After examining the flow dynamics of viscoelastic fluids inside contraction geometries, the characteristics of transient state, before reaching steady state, were studied. The primary purpose of this part was to compare the transient start-up flow at high $Wi$ with the steady state flows at lower $Wi$. The development of the flow pattern from a Newtonian-like to corner vortex was observed as $Wi$ increased at steady states. Depending on the type of the fluid and channel size, the flow sequence was different. However, in all the cases we could cover including the numerical simulation, the flow patterns of the early-phase transient flow with a high $Wi$ matched well with the flow patterns of the steady states with a low $Wi$. In other words, it was possible to match the steady flow patterns with a low $Wi$ flows and the transient patterns with a high $Wi$ flow. The plot of $Wi$ and time when the two sets (steady and transient) were matched followed a similar form regardless of the type of fluid and channel dimension used, and the slope changed significantly at the point when the corner vortex first appeared. From this fact, it could be confirmed that there

exists a special relationship between time and elasticity, called time-$Wi$ superposition in the vortex dynamics of viscoelastic fluids in the contraction flow. It is impressive that there exists a simple principle that dominates the complex flow behavior of viscoelastic fluids in the contraction channel flow.


**Unstable flows**


In the last part, the unsteady state was systemically analyzed. To reach the unstable states, only one kind of geometry (200 μm: 50 μm) and highly elastic fluids ($M_w$=5×10$^6$ g mol$^{-1}$) were used. The development sequence of the flow pattern over increasing elasticity numbers ($El$) or Weissenberg numbers ($Wi$) was organized again with those highly elastic fluids. In the steady state, the sequence of the flow development started with a Newtonian-like flow, and became a divergent flow where the streamlines were distorted and the maximum flow velocity occurring not at the contraction but further upstreamLastly, vortex formation occurred. Depending on the fluid, small vortices may develop before the divergent flow and disappear. This was named as a weak vortex while the vortex that occurred after the divergent flow was vortex growth region. In the vortex growth region, the vortex size increased with the increase in $Wi$. As $El$ or $Wi$ increased, the flow reached unsteady state. While the flow patterns were maintained over time in the steady state, it changed continuously in the unsteady state. The vortex size in the vortex growth region was constant and stable at a specific $Wi$. However, as the $Wi$ increased, the vortex started to fluctuate

periodically. This was called an oscillating vortex. Right after the flow transitioned into the unsteady state, the vortex on both sides oscillated symmetrically. At a higher $Wi$, the asymmetric oscillation was observed. While only one pattern of vortex dynamics was observed for the symmetric oscillating vortex, the asymmetric oscillating vortex showed different patterns with a difference in vortex size for the two vortices but with a single period. When $Wi$ increased over the asymmetric oscillating vortex region, the periodicity of the vortex fluctuation disappeared. In this aperiodic fluctuation regime, the largest Lyapunov exponent was positive, which proves that the vortex behavior is chaotic. The flow patterns in micro-contraction geometry were systematically analyzed in this study, and the chaotic vortex dynamics were reported for the first time.

# REFERENCES

Afonso, A. M., Oliveira, P. J., Pinho, F. T., & Alves, M. A. (2011). Dynamics of high-Deborah-number entry flows: a numerical study. *Journal of Fluid Mechanics*, *677*, 272-304.

Alves, M. A., Pinho, F. T., & Oliveira, P. J. (2005). Visualizations of Boger fluid flows in a 4: 1 square–square contraction. *AIChE journal*, *51*(11), 2908-2922.

Alves, M. A., Pinho, F. T., & Oliveira, P. J. (2008). Viscoelastic flow in a 3D square/square contraction: visualizations and simulations. *Journal of Rheology (1978-present)*, *52*(6), 1347-1368.

Alves, M. A., & Poole, R. J. (2007). Divergent flow in contractions. *Journal of non-newtonian fluid mechanics*, *144*(2), 140-148.

Anderson, J. R., Chiu, D. T., Wu, H., Schueller, O. J., & Whitesides, G. M. (2000). Fabrication of microfluidic systems in poly (dimethylsiloxane).*Electrophoresis*, *21*, 27-40.

Bishko, G. B., Harlen, O. G., McLeish, T. C. B., & Nicholson, T. M. (1999). Numerical simulation of the transient flow of branched polymer melts through a planar contraction using thepom–pom'model. *Journal of non-newtonian fluid mechanics*, *82*(2), 255-273.

Boger, D. V. (1987). Viscoelastic flows through contractions. *Annual review of fluid mechanics*, *19*(1), 157-182.

Boger, D. V., & Walters, K. (1993). *Rheological phenomena in focus*. Elsevier.

Boger, D. V., Hur, D. U., & Binnington, R. J. (1986). Further observations of elastic effects in tubular entry flows. *Journal of Non-Newtonian Fluid Mechanics*,*20*, 31-49.

Bonn, D., & Meunier, J. (1997). Viscoelastic free-boundary problems: Non-newtonian viscosity vs normal stress effects. *Physical review letters*, *79*(14), 2662.

Cable, P. J., & Boger, D. V. (1978). A comprehensive experimental investigation of tubular entry flow of viscoelastic fluids: Part I. Vortex characteristics in stable flow. *AIChE Journal*, *24*(5), 869-879.

Cable, P. J., & Boger, D. V. (1978). A comprehensive experimental investigation of tubular entry flow of viscoelastic fluids. Part II. The velocity field in stable flow.*AIChE Journal*, *24*(6), 992-999.

Cable, P. J., & Boger, D. V. (1979). A comprehensive experimental investigation of tubular entry flow of viscoelastic fluids: Part III. Unstable flow. *AIChE Journal*,*25*(1), 152-159.

Chiba, K., Tanaka, S., & Nakamura, K. (1992). The structure of anomalous entry flow patterns through a planar contraction. *Journal of non-newtonian fluid mechanics*, *42*(3), 315-322.

Chiba, K., Ishida, R., & Nakamura, K. (1995). Mechanism for entry flow instability through a forward-facing step channel. *Journal of non-newtonian fluid mechanics*, *57*(2), 271-282.

Cogswell, F. N. (1972). Converging flow of polymer melts in extrusion dies.*Polymer Engineering & Science*, *12*(1), 64-73.

Dembek, G. (1982). Structural changes of polyisobutylene solutions induced by orifice flow. In *Progress and Trends in Rheology* (pp. 199-201). Steinkopff.

Dendukuri, D., Gu, S. S., Pregibon, D. C., Hatton, T. A., & Doyle, P. S. (2007). Stop-flow lithography in a microfluidic device. *Lab on a Chip*, *7*(7), 818-828.

Devasenathipathy, S., Santiago, J. G., Wereley, S. T., Meinhart, C. D., & Takehara, K. (2003). Particle imaging techniques for microfabricated fluidic systems. *Experiments in Fluids*, *34*(4), 504-514.

Evans, R. E., & Walters, K. (1986). Flow characteristics associated with abrupt changes in geometry in the case of highly elastic liquids. *Journal of Non-Newtonian Fluid Mechanics*, *20*, 11-29.

Evans, R. E., & Walters, K. (1989). Further remarks on the lip-vortex mechanism of vortex enhancement in planar-contraction flows. *Journal of non-newtonian fluid mechanics*, *32*(1), 95-105.

Groisman, A., & Steinberg, V. (1998). Elastic vs. inertial instability in a polymer solution flow. *EPL (Europhysics Letters)*, *43*(2), 165.

Groisman, A., & Quake, S. R. (2004). A microfluidic rectifier: anisotropic flow resistance at low Reynolds numbers. *Physical review letters*, *92*(9), 094501.

Gulati, S., Muller, S. J., & Liepmann, D. (2008). Direct measurements of viscoelastic flows of DNA in a 2: 1 abrupt planar micro-contraction. *Journal of Non-Newtonian Fluid Mechanics*, *155*(1), 51-66.

Haste, F.V. (2007) Troubleshooter: Extrusion – Stop black specks!, *Plastics Technology*.

Hertel, D., & Münstedt, H. (2008). Dependence of the secondary flow of a low-density polyethylene on processing parameters as investigated by laser-Doppler velocimetry. *Journal of Non-Newtonian Fluid Mechanics*, *153*(2), 73-81.

Kang, K., Lee, L. J., & Koelling, K. W. (2005). High shear microfluidics and its application in rheological measurement. *Experiments in fluids*, *38*(2), 222-232.

Kim, J. M., Chung, C., Ahn, K. H., & Jong, L. S. (2005). Time-weissenberg number superposition in 4: 1 planar contraction flow of a viscoelastic fluid. 日本レオロジー学会誌, *33*(4), 191-197.

Kwon, Y. (2012). Numerical description of elastic flow instability and its dependence on liquid viscoelasticity in planar contraction. *Journal of Rheology (1978-present)*, *56*(6), 1335-1362.

Kwon, Y., & Park, K. S. (2012). Decoupled algorithm for transient viscoelastic flow modeling. *Korea-Australia Rheology Journal*, *24*(1), 53-63.

Lawler, J. V., Muller, S. J., Brown, R. A., & Armstrong, R. C. (1986). Laser Doppler velocimetry measurements of velocity fields and transitions in viscoelastic fluids. *Journal of Non-Newtonian Fluid Mechanics*, *20*, 51-92.

McDonald, J. C., & Whitesides, G. M. (2002). Poly (dimethylsiloxane) as a material for fabricating microfluidic devices. *Accounts of chemical research*,*35*(7), 491-499.

McKinley, G. H., Raiford, W. P., Brown, R. A., & Armstrong, R. C. (1991). Nonlinear dynamics of viscoelastic flow in axisymmetric abrupt contractions.*Journal of Fluid Mechanics*, *223*, 411-456.

McKinley, G. H., Rodd, L. E., Oliverira, M. S., & Cooper-White, J. (2007). Extensional flows of polymer solutions in microfluidic converging/diverging geometries. *Journal of Central South University of Technology*, *14*(1), 6-9.

Meinhart, C. D., Wereley, S. T., & Santiago, J. G. (1999). PIV measurements of a

microchannel flow. *Experiments in Fluids*, *27*(5), 414-419.

Mitchell, P. (2001). Microfluidics-downsizing large-scale biology. *Nature biotechnology*, *19*(8), 717-721.

Nigen, S., & Walters, K. (2002). Viscoelastic contraction flows: comparison of axisymmetric and planar configurations. *Journal of non-newtonian fluid mechanics*, *102*(2), 343-359.

Nguyen, H., & Boger, D. V. (1979). The kinematics and stability of die entry flows. *Journal of Non-Newtonian Fluid Mechanics*, *5*, 353-368.

Oliveira, M. S. N., Alves, M. A., Pinho, F. T., & McKinley, G. H. (2007). Viscous flow through microfabricated hyperbolic contractions. *Experiments in fluids*, *43*(2-3), 437-451.

Owens, R. G., & Phillips, T. N. (2002). *Computational rheology* (Vol. 2, No. 2). London: Imperial College Press.

Pakdel, P., & McKinley, G. H. (1996). Elastic instability and curved streamlines. *Physical review letters*, *77*(12), 2459.

Raffel, M., Willert, C.E., Kompenhans, J., Particle image velocimetry, *Springer* (1998).

Scott, T. P. (2004). *Contraction/expansion flow of dilute elastic solutions in microchannels* (Doctoral dissertation, Massachusetts Institute of Technology).

Raiford, W. P., Quinzani, L. M., Coates, P. J., Armstrong, R. C., & Brown, R. A. (1989). LDV measurements of viscoelastic flow transitions in abrupt axisymmetric contractions: interaction of inertia and elasticity. *Journal of non-newtonian fluid mechanics*, *32*(1), 39-68.

Rodd, L.E. (2006) Planar entry flow of low viscosity elastic fluids in microfabricated

contraction geometires, *Ph.D. Thesis*, The University of Melbourne.

Rodd, L. E., Cooper-White, J. J., Boger, D. V., & McKinley, G. H. (2007). Role of the elasticity number in the entry flow of dilute polymer solutions in micro-fabricated contraction geometries. *Journal of Non-Newtonian Fluid Mechanics*,*143*(2), 170-191.

Rodd, L. E., Lee, D., Ahn, K. H., & Cooper-White, J. J. (2010). The importance of downstream events in microfluidic viscoelastic entry flows: Consequences of increasing the constriction length. *Journal of Non-Newtonian Fluid Mechanics*,*165*(19), 1189-1203.

Rodd, L. E., Scott, T. P., Boger, D. V., Cooper-White, J. J., & McKinley, G. H. (2005). The inertio-elastic planar entry flow of low-viscosity elastic fluids in micro-fabricated geometries. *Journal of Non-Newtonian Fluid Mechanics*, *129*(1), 1-22.

Rodd, L. E., Scott, T. P., Cooper-White, J. J., & McKinley, G. H. (2004). Capillary break-up rheometry of low-viscosity elastic fluids. Applied Rheology 15 (1)

Rothstein, J. P., & McKinley, G. H. (2001). The axisymmetric contraction–expansion: the role of extensional rheology on vortex growth dynamics and the enhanced pressure drop. *Journal of non-newtonian fluid mechanics*, *98*(1), 33-63.

Rosenstein, M. T., Collins, J. J., & De Luca, C. J. (1993). A practical method for calculating largest Lyapunov exponents from small data sets. *Physica D: Nonlinear Phenomena*, *65*(1), 117-134.

Santiago, J. G., Wereley, S. T., Meinhart, C. D., Beebe, D. J., & Adrian, R. J. (1998). A particle image velocimetry system for microfluidics. *Experiments in fluids*, *25*(4), 316-319.

Schuberth, S., & Münstedt, H. (2008). Transient elongational viscosities of aqueous

polyacrylamide solutions measured with an optical rheometer.*Rheologica Acta*, *47*(2), 139-147.

Sousa, P. C., Pinho, F. T., Oliveira, M. S. N., & Alves, M. A. (2011). Extensional flow of blood analog solutions in microfluidic devices.*Biomicrofluidics*, *5*(1), 014108.

Sprott, J. C., & Sprott, J. C. (2003). *Chaos and time-series analysis* (Vol. 69). Oxford: Oxford University Press.

Stroock, A. D., & Whitesides, G. M. (2002). Components for integrated poly (dimethylsiloxane) microfluidic systems. *Electrophoresis*, *23*(20), 3461-73.

Szabo, P., Rallison, J. M., & Hinch, E. J. (1997). Start-up of flow of a FENE-fluid through a 4: 1: 4 constriction in a tube. *Journal of non-newtonian fluid mechanics*, *72*(1), 73-86.

Viriyayuthakorn, M., & Caswell, B. (1980). Finite element simulation of viscoelastic flow. *Journal of Non-Newtonian Fluid Mechanics*, *6*(3), 245-267.

Walters, K., & Webster, M. F. (1982). On dominating elastico-viscous response in some complex flows. *Philosophical Transactions of the Royal Society of London. Series A, Mathematical and Physical Sciences*, *308*(1502), 199-218.

Walters, K., & Rawlinson, D. M. (1982). On some contraction flows for Boger fluids. In *Progress and Trends in Rheology* (pp. 193-198). Steinkopff.

Wereley, S. T., & Meinhart, C. D. (2005). Micron-resolution particle image velocimetry. In *Microscale Diagnostic Techniques* (pp. 51-112). Springer Berlin Heidelberg.

White, S. A., Gotsis, A. D., & Baird, D. G. (1987). Review of the entry flow problem: experimental and numerical. *Journal of non-newtonian fluid mechanics*, *24*(2), 121-

160.

Whitesides, G. M. (2006). The origins and the future of microfluidics. *Nature*,*442*(7101), 368-373.

Whitesides, G., & Stroock, A. (2001). Flexible methods for microfluidics [J].*Phys Today*, *54*(6), 42-48.

Yasuda, K., & Sugiura, Y. (2008). Entry Flows of Polymer Solutions through a Planar Contraction in a Microchannel. *Journal of Fluid Science and Technology*,*3*, 987-998.

Yesilata, B., Ö ztekin, A., & Neti, S. (1999). Instabilities in viscoelastic flow through an axisymmetric sudden contraction. *Journal of non-newtonian fluid mechanics*, *85*(1), 35-62.

Yesilata, B., Ö ztekin, A., & Neti, S. (2000). Non-isothermal viscoelastic flow through an axisymmetric sudden contraction. *Journal of non-newtonian fluid mechanics*, *89*(1), 133-164.

# 국문 요약

# 4:1 수축 미세 유로를 흐르는

# 탄성 유체의 흐름에 관한 연구

이대웅

서울대학교 대학원

화학생물공학부

수축 유로를 흐르는 점탄성 유체의 구조는 유변학의 관심 연구 분야 중 하나이다. 특히, 와류의 형성은 매우 중요한 문제이다. 와류는 고분자 가공 공정과 같은 실용적인 사용에 있어서 바람직하지 않은 현상이다. 이는 물질의 체류 시간을 증가시킴으로써 최종 제품 불량을 초래하기 때문이다. 따라서 이를 이해하기 위해 와류 거동에 대한 많은 연구가 있어 왔다. 그러나 수축 유로에서 순수하게 탄성으로 인해 발생하는 흐름 거동에 대한 관심은 적었으며, 특히 탄성으로 인한 비정상상태 흐름에 대해서는 더욱 그러했다. 본 논문에서는 탄성으로 인해 발생하는 흐름의 형태가 어떻게 변화하는지를 살폈다. 그에 더해 정상상태에

도달하기까지의 전이 상태에서 발생하는 현상과 탄성의 증가로 인하여 정상상태에서 벗어났을 때 흐름이 어떻게 거동하는지를 연구하였다.

본 연구는 세 가지 목적이 있다. 첫 번째 목적은 수축 유로를 흐르는 탄성 흐름의 구조를 알아내는 것이다. 이에 4:1 평면 직각 수축 미세 유로를 흐르는 점탄성 유체의 흐름 형태를 관찰하고 정량적으로 분석하였다. 미세하게 제작된 장치의 경우 그 작은 크기로 인해 탄성으로 인한 효과를 증가시키며, 또한 고해상도의 가시화 기법을 이용하여 흐름을 관찰하기에 용이하다. 폴리에틸렌 옥사이드 용액으로 낮은 레이놀즈 수($Re$)를 유지하면서도($O(10^{-2})$>Re) 넓은 범위의 와이젠버그 수($Wi$)에서 그 흐름을 관찰하였다. 흐름 형태는 특별한 특징이 없는 흐름에서부터, divergent 흐름, lip 와류, corner 와류 등의 과정을 지나 와류가 자라나는 것이 관찰되었으며, 이는 탄성 수($El$)와 채널의 종횡비에 영향을 받는다. 탄성 수와 채널 종횡비에 따라서 수축 미세유로를 흐르는 흐름의 형태는 다양한 형태로 발전한다는 것이 발견되었다. (3 장)

두 번째 목적은 높은 $Wi$ 를 갖는 흐름의 초기 전이 흐름과 그보다 낮은 $Wi$ 를 갖는 흐름의 정상 상태 흐름의 관계를 파악하여

시간$-Wi$ 중첩을 실험적으로 수립하는 것이다. $Wi$ 가 증가하면서 흐름은 뉴턴유체와 같은 흐름에서부터 발전하여 와류가 성장하게 되는데, 높은 $Wi$ 를 갖는 흐름의 초기 전이 상태 흐름은 정상 상태에 도달하기까지 그보다 낮은 $Wi$ 를 갖는 흐름이 보이는 모든 정상 상태 흐름 형태를 경험한다. 상술했던 것처럼 흐름의 발전 과정은 유로나 유체에 영향을 받지만, 그 모든 상황에서도 높은 $Wi$ 의 초기 흐름과 그보다 낮은 $Wi$ 의 정상 상태 흐름들은 1:1 로 비교 가능하다. 이러한 비교를 통해 $Wi$ 와 시간으로 (전이 상태 흐름 대 정상 상태 흐름) 그래프를 그리면, 독특한 패턴이 나타나며, 이로써 시간$-Wi$ 중첩을 증명할 수 있다. (4 장)

논문의 마지막 장에서는, 비정상상태 흐름의 성질을 분석하였다. 3 장과 4 장에서는 정상 상태 흐름을 다루었다. 하지만 전단 속도의 증가 혹은 유체의 탄성의 증가로 인해 $Wi$ 가 증가하면, 와류는 특정한 주기를 가지고 출렁이게 된다. 이러한 비정상 상태에 도달하기 위하여 높은 탄성을 가진 유체를 (분자량 500 만의 폴리에틸렌 옥사이드 용액) 사용하였다. 비정상상태 흐름에서 와류는 끊임없이 출렁인다. 먼저 이는 특정한 주기를 가지고 출렁이는데, 이를 주기성 와류라고 한다. 이런 주기성

와류는 처음에 대칭으로 출렁이다가 탄성이 증가하면서 다양한 형태를 갖는 비대칭 주기성 와류가 된다. 탄성이 더욱 증가하면 주기성은 사라지고 무작위로 출렁이게 된다. 이렇게 무작위로 출렁이는 영역에서 와류의 크기로 그래프를 그려 리야프노프 지수를 구한 결과 양수이며, 이는 와류의 출렁임이 공간적으로 무질서함을 나타낸다. (5 장)

본 논문에서는 미세하게 제작된 수축 유로를 흐르는 탄성 유체의 흐름 형태를 세밀하게 분석하였다. 분석한 흐름 형태에는 뉴턴 유체와 같이 별다른 특징이 없는 흐름, divergent 흐름, 정상상태에서의 와류 성장, 대칭형 주기성 와류, 비대칭형 주기성 와류, 무질서한 흐름 등이 있다.